2003

Kinematically Complete Measurement of the Proton Structure Function F₂ in the Resonance Region and Evaluation of its Moments

M. Bektasoglu
Old Dominion University

L. Ciciani
Old Dominion University

K. V. Dharmawardane
Old Dominion University

G. E. Dodge
Old Dominion University, gdodge@odu.edu

C. E. Hyde-Wright
Old Dominion University, chyde@odu.edu

Original Publication Citation

Authors

M. Bektasoglu, L. Ciciani, K. V. Dharmawardane, G. E. Dodge, C. E. Hyde-Wright, A. Klein, A. V. Klimenko, S. E. Kuhn, F. Sabatié, S. Stepanyan, L. B. Weinstein, J. Yun, et al., and CLAS Collaboration

Kinematically complete measurement of the proton structure function F_2 in the resonance region and evaluation of its moments

M. Osipenko,[1,2] G. Ricco,[2] M. Taiuti,[2] M. Ripani,[2] S. Simula,[3] G. Adams,[4] E. Anciant,[5] M. Anghinolfi,[2] B. Asavapibhop,[7] G. Audit,[5] T. Auger,[5] H. Avakian,[8,9] H. Bagdasaryan,[10] J. P. Ball,[11] S. Barrow,[24] M. Battaglieri,[2] K. Beard,[31] M. Bektasoglu,[20] N. Bianchi,[9] A. S. Biselli,[4] S. Boiarinov,[8,35] P. Bosted,[7] S. Bouchigny,[12,8] R. Bradford,[17] D. Branford,[13] W. J. Briscoe,[14] W. K. Brooks,[8] V. D. Burkert,[8] J. R. Calarco,[15] D. S. Carman,[16] B. Carnahan,[18] A. Cazes,[19] C. Cetina,[14,17] L. Ciciani,[20] R. Clark,[17] P. L. Cole,[21,8] A. Coleman,[6,*] D. Cords,[8,†] P. Corvisiero,[2] D. Crabb,[22] H. Crannell,[18] J. P. Cummings,[4] E. De Sanctis,[9] P. V. Degtyarenko,[8] H. Denizli,[23] L. Dennis,[24] R. De Vita,[2] K. V. Dharmawardane,[20] C. Djalali,[19] G. E. Dodge,[20] J. J. Domingo,[8] D. Doughty,[25,8] P. Dragovitsch,[24] M. Dugger,[11] S. Dytman,[23] M. Eckhause,[6] H. Egiyan,[6] K. S. Egiyan,[10] L. Elouadrhiri,[8] A. Empl,[4] R. Fatemi,[22] G. Fedotov,[1] R. J. Feuerbach,[17] J. Ficenec,[26] T. A. Forest,[20] H. Funsten,[6] S. J. Gaff,[27] M. Gai,[28] G. Gavalian,[15,10] S. Gilad,[29] G. P. Gilfoyle,[30] K. L. Giovanetti,[31] P. Girard,[19] K. Griffioen,[6] E. Golovatch,[1] C. I. O Gordon,[32] M. Guidal,[12] M. Guillo,[19] L. Guo,[8] V. Gyurjyan,[8] C. Hadjidakis,[12] J. Hardie,[25,8] D. Heddle,[25,8] F. W. Hersman,[15] K. Hicks,[16] R. S. Hicks,[7] M. Holtrop,[15] J. Hu,[4] C. E. Hyde-Wright,[20] B. S. Ishkhanov,[1] M. M. Ito,[8] D. Jenkins,[26] K. Joo,[8,22] J. H. Kelley,[27] J. D. Kellie,[32] M. Khandaker,[33] D. H. Kim,[34] K. Y. Kim,[23] K. Kim,[34] M. S. Kim,[34] W. Kim,[34] A. Klein,[20] F. J. Klein,[18,8] A. V. Klimenko,[20] M. Klusman,[4] M. Kossov,[35] L. H. Kramer,[37,8] Y. Kuang,[6] S. E. Kuhn,[20] J. Kuhn,[4] J. Lachniet,[17] J. M. Laget,[5] D. Lawrence,[7] Ji Li,[4] K. Livingston,[32] K. Lukashin,[8,18] J. J. Manak,[8] C. Marchand,[5] S. McAleer,[24] J. McCarthy,[22] J. W. C. McNabb,[17] B. A. Mecking,[8] S. Mehrabyan,[23] M. D. Mestayer,[8] C. A. Meyer,[17] K. Mikhailov,[35] R. Minehart,[22] M. Mirazita,[9] R. Miskimen,[7] V. Mokeev,[1,8] L. Morand,[5] S. A. Morrow,[12,5] V. Muccifora,[9] J. Mueller,[23] L. Y. Murphy,[14] G. S. Mutchler,[36] J. Napolitano,[4] R. Nasseripour,[37] S. O. Nelson,[27] S. Niccolai,[14] G. Niculescu,[16] I. Niculescu,[14] B. B. Niczyporuk,[8] R. A. Niyazov,[20] M. Nozar,[8,33] G. V. O'Rielly,[14] A. K. Opper,[16] K. Park,[34] K. Paschke,[17] E. Pasyuk,[11] G. Peterson,[7] S. A. Philips,[14] N. Pivnyuk,[35] D. Pocanic,[22] O. Pogorelko,[35] E. Polli,[9] S. Pozdniakov,[35] B. M. Preedom,[19] J. W. Price,[38] Y. Prok,[22] D. Protopopescu,[32] L. M. Qin,[20] B. A. Raue,[37,8] G. Riccardi,[24] B. G. Ritchie,[11] F. Ronchetti,[9,3] P. Rossi,[9] D. Rowntree,[29] P. D. Rubin,[30] F. Sabatié,[5,20] K. Sabourov,[27] C. Salgado,[33] J. P. Santoro,[26,8] V. Sapunenko,[8] M. Sargsyan,[37,8] R. A. Schumacher,[17] V. S. Serov,[35] Y. G. Sharabian,[8,10] J. Shaw,[7] S. Simionatto,[14] A. V. Skabelin,[29] E. S. Smith,[8] L. C. Smith,[22] D. I. Sober,[18] M. Spraker,[27] A. Stavinsky,[35] S. Stepanyan,[20,10] P. Stoler,[4] S. Taylor,[36] D. J. Tedeschi,[19] U. Thoma,[8] R. Thompson,[23] L. Todor,[17] C. Tur,[19] M. Ungaro,[4] M. F. Vineyard,[30,‡] A. V. Vlassov,[35] K. Wang,[22] L. B. Weinstein,[20] H. Weller,[27] D. P. Weygand,[8] C. S. Whisnant,[19,31] E. Wolin,[8] M. H. Wood,[19] A. Yegneswaran,[8] J. Yun,[20] B. Zhang,[29] J. Zhao,[29] and Z. Zhou[29,25]

(CLAS Collaboration)

[1]*Moscow State University, 119992 Moscow, Russia*
[2]*INFN, Sezione di Genova, and Dipartimento di Fisica dell'Università, 16146 Genova, Italy*
[3]*Università di ROMA III, 00146 Roma, Italy*
[4]*Rensselaer Polytechnic Institute, Troy, New York 12180*
[5]*CEA-Saclay, Service de Physique Nucléaire, F91191 Gif-sur-Yvette, Cedex, France*
[6]*College of William and Mary, Williamsburg, Virginia 23187*
[7]*University of Massachusetts, Amherst, Massachusetts 01003*
[8]*Thomas Jefferson National Accelerator Facility, Newport News, Virginia 23606*
[9]*INFN, Laboratori Nazionali di Frascati, PO 13, 00044 Frascati, Italy*
[10]*Yerevan Physics Institute, 375036 Yerevan, Armenia*
[11]*Arizona State University, Tempe, Arizona 85287*
[12]*Institut de Physique Nucleaire ORSAY, IN2P3 BP 1, 91406 Orsay, France*
[13]*Edinburgh University, Edinburgh EH9 3JZ, United Kingdom*
[14]*The George Washington University, Washington, DC 20052*
[15]*University of New Hampshire, Durham, New Hampshire 03824*
[16]*Ohio University, Athens, Ohio 45701*
[17]*Carnegie Mellon University, Pittsburgh, Pennsylvania 15213*
[18]*Catholic University of America, Washington, D.C. 20064*
[19]*University of South Carolina, Columbia, South Carolina 29208*
[20]*Old Dominion University, Norfolk, Virginia 23529*
[21]*University of Texas at El Paso, El Paso, Texas 79968*
[22]*University of Virginia, Charlottesville, Virginia 22901*
[23]*University of Pittsburgh, Pittsburgh, Pennsylvania 15260*

*Current address: Systems Planning and Analysis, Alexandria, VA 22311.

†Deceased.

‡Current address: Union College, Schenectady, NY 12308.

^{24}*Florida State University, Tallahassee, Florida 32306*
^{25}*Christopher Newport University, Newport News, Virginia 23606*
^{26}*Virginia Polytechnic Institute and State University, Blacksburg, Virginia 24061*
^{27}*Duke University, Durham, North Carolina 27708*
^{28}*University of Connecticut, Storrs, Connecticut 06269*
^{29}*Massachusetts Institute of Technology, Cambridge, Massachusetts 02139*
^{30}*University of Richmond, Richmond, Virginia 23173*
^{31}*James Madison University, Harrisonburg, Virginia 22807*
^{32}*University of Glasgow, Glasgow G12 8QQ, United Kingdom*
^{33}*Norfolk State University, Norfolk, Virginia 23504*
^{34}*Kyungpook National University, Taegu 702-701, South Korea*
^{35}*Institute of Theoretical and Experimental Physics, Moscow, 117259, Russia*
^{36}*Rice University, Houston, Texas 77005*
^{37}*Florida International University, Miami, Florida 33199*
^{38}*University of California at Los Angeles, Los Angeles, California 90095*

We measured the inclusive electron-proton cross section in the nucleon resonance region ($W<2.5$ GeV) at momentum transfers Q^2 below 4.5 (GeV/c)^2 with the CLAS detector. The large acceptance of CLAS allowed the measurement of the cross section in a large, contiguous two-dimensional range of Q^2 and x, making it possible to perform an integration of the data at fixed Q^2 over the significant x interval. From these data we extracted the structure function F_2 and, by including other world data, we studied the Q^2 evolution of its moments, $M_n(Q^2)$, in order to estimate higher twist contributions. The small statistical and systematic uncertainties of the CLAS data allow a precise extraction of the higher twists and will require significant improvements in theoretical predictions if a meaningful comparison with these new experimental results is to be made.

I. INTRODUCTION

The striking features of the nucleon structure function F_2 were first noted nearly 30 years ago by Bloom and Gilman [1]. They empirically observed two effects in data measured at SLAC: (a) the dual behavior of the $F_2(x,Q^2)$ function that shows common features between the two kinematic regions corresponding to the nucleon resonances and deep inelastic scattering (DIS); (b) the extension of the scaling region to lower Q^2 values when $F_2(x',Q^2)$ is plotted as a function of $x'=x/(1+M^2x^2/Q^2)$, the "improved scaling variable." More precisely, they found that the smooth function $F_2(x')$ measured at high Q^2 in the DIS region represents a good average over the resonances of the $F_2(x',Q^2)$ structure function measured at lower Q^2 values. Moreover, the duality appears to be valid locally. In fact, each of the most prominent resonance bumps, when averaged within its width, shows approximate scaling [2]. Later on, in the framework of QCD, De Rujula, Georgi and Politzer [3] provided the first explanation of the Bloom-Gilman duality. They evaluated the Cornwall-Norton [4] moments $M_n^{CN}(Q^2)$ of the nucleon structure function F_2, defined as

$$M_n^{CN}(Q^2)=\int_0^1 dx\, x^{(n-2)}F_2(x,Q^2),\qquad(1)$$

and using the operator product expansion (OPE) they obtained the following expression:

$$M_n^{CN}(Q^2)=A_n(Q^2)+\sum_{k=1}^{\infty}\left(n\frac{\gamma^2}{Q^2}\right)^k B_{nk}(Q^2),\qquad(2)$$

where $A_n(Q^2)$ can be evaluated in the framework of perturbative QCD (PQCD), and it is directly connected to the corresponding moment of the asymptotic limit of F_2. The contribution of the higher twists, which is related to multi-parton correlations inside the nucleon and represented by $B_{nk}(Q^2)$, depends on the value of the constant γ^2 in such a way that γ^2 can be considered as a scale constant for higher twist effects. Assuming a small value of the constant γ^2, the authors of Ref. [3] showed that the contribution of the higher twists was relatively small, at least for low values of n and for $Q^2 \gtrsim M^2$, justifying the observed dual behavior of the structure function.

It is now well established that the interpretation of the parton-hadron duality in light of QCD requires the evaluation of the moments of the nucleon structure functions and their evolution as a function of Q^2. Current PQCD calculations can estimate the Q^2 evolution up to the next-to-next-to-leading order, giving access to the interesting kinematic region of high x and moderate Q^2 where the multi-parton correlation contribution to the nucleon wave function becomes dominant.

The interest in investigating multi-parton correlations in inelastic lepton scattering off the nucleon at large values of x has recently been renewed, leading to a re-analysis of old F_2 data [5,6]. Unfortunately, the results from Refs. [5] and [6] were mainly based on the analysis of fits of the structure function F_2 and therefore were still qualitative. Moreover, the previous lack of data in the resonance region did not allow a model independent evaluation of the moment evolution to lower Q^2, and therefore offered very few opportunities to quantitatively investigate the role of QCD below the DIS limit.

The Hall C Collaboration at the Thomas Jefferson National Accelerator Facility (TJNAF) has recently provided high quality data in this kinematic region [7], allowing a more precise evaluation of the moments of the F_2 structure function of the proton [2]. However, like many other such measurements, the data were taken with a spectrometer of relatively small angular acceptance and the measured inclusive cross sections do not span a large continuous x interval for constant Q^2. Data taken in this manner follow a kinematic locus in Q^2 vs x and require substantial interpolation to determine the F_2 moments.

In this paper we report the first measurement in a wide continuous interval in x and Q^2 (see Fig. 1) of the inclusive electron-proton scattering cross section. These measurements were performed at TJNAF with the CLAS detector in Hall B. The F_2 structure function was extracted over the whole resonance region ($W \leq 2.5$ GeV) below $Q^2 = 4.5$ (GeV/c)^2. This measurement, together with existing world data, allowed for the evaluation of the F_2 moments, drastically reducing the uncertainties related to data interpolation and providing the most detailed dependence on Q^2 of the moments up to $n = 8$. Furthermore, the elastic contribution to the moments was updated with respect to Ref. [5] using the fit of the nucleon form factors from Ref. [8] adjusted to the Jefferson Lab data on the ratio G_E/G_M [9], as described in Ref. [10]. Finally, we used our new determination of the F_2 moments to extract the higher twist contribution as a function of Q^2.

In Sec. II we review the F_2 moments in the framework of PQCD. In Sec. III we discuss the analysis of the data, including the extraction of the F_2 structure function from the cross section. The evaluation of the moments and uncertainties is also presented in Sec. III. Finally, Sec. IV is devoted to the interpretation of the results.

II. MOMENTS OF THE STRUCTURE FUNCTION F_2

Until recently the studies of inclusive lepton-nucleon scattering represented the main source of information about nucleon structure. In the DIS region, measured structure functions can be directly connected to the parton momentum distribution of the nucleon in the framework of PQCD. After the successful interpretation of the DIS region, the intermediate kinematic domain, situated at Q^2 of a few (GeV/c)^2 and large values of x, attracted the interest of physicists. Despite interpretation difficulties, this region allows the study of multi-parton correlation contribution to the proton wave function. These processes are not accessible in DIS due to the small value of the running coupling constant $\alpha_S(Q^2)$.

The OPE of the virtual photon-nucleon scattering amplitude leads to the description of the complete Q^2 evolution of the moments of the nucleon structure functions. The nth Cornwall-Norton moment [4] of the (asymptotic) structure function $F_2(x,Q^2)$ for a massless nucleon can be expanded as

$$M_n^{CN}(Q^2) = \sum_{\tau=2k}^{\infty} E_{n\tau}(\mu,Q^2) O_{n\tau}(\mu) \left(\frac{\mu^2}{Q^2}\right)^{(\tau-2)/2}, \quad (3)$$
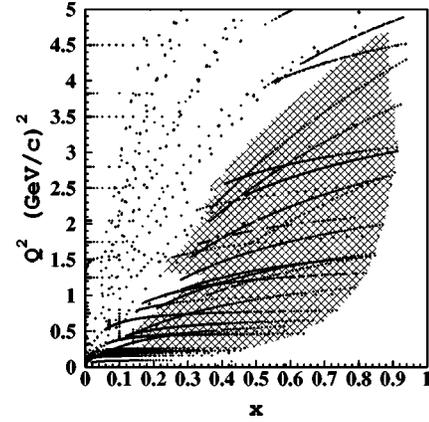
FIG. 1. Experimental data on the structure function $F_2(x,Q^2)$ used for the moment evaluation in the CLAS kinematic region: points, world data; shaded area, CLAS data.

where $k = 1, 2, \ldots, \infty$, μ is the factorization scale, $O_{n\tau}(\mu)$ is the reduced matrix element of the local operators with definite spin n and twist τ (dimension minus spin), related to the non-perturbative structure of the target. $E_{n\tau}(\mu,Q^2)$ is a dimensionless coefficient function describing the small distance behavior, which can be perturbatively expressed as a power expansion of the running coupling constant $\alpha_s(Q^2)$.

At Q^2 values comparable with the squared proton mass, M^2, the structure function F_2 still contains non-negligible mass-dependent terms that produce in Eq. (3) additional M^2/Q^2 power corrections (kinematic twists). To avoid these terms, the moments $M_n^{CN}(Q^2)$ of the massless F_2 have to be replaced in Eq. (3) by the corresponding Nachtmann [11] moments $M_n^N(Q^2)$ of the measured structure function $F_2(x,Q^2)$ (see also Ref. [12]). It has been shown that

$$M_n^{CN}(F_2^{lim}(x,Q^2)) = M_n^N(F_2(x,Q^2)), \quad (4)$$

where $F_2^{lim}(x,Q^2)$ is the asymptotic structure function of the massless nucleon and

$$M_n^N(Q^2) = \int_0^1 dx \frac{\xi^{n+1}}{x^3} F_2(x,Q^2)$$

$$\times \left[\frac{3 + 3(n+1)r + n(n+2)r^2}{(n+2)(n+3)} \right], \quad (5)$$

where $r = \sqrt{1 + 4M^2 x^2/Q^2}$ and $\xi = 2x/(1+r)$.

Since the moments in Eq. (3) are totally inclusive, the elastic contribution at $x = 1$ has to be added according to Ref. [2]:

$$F_2^{el}(x,Q^2) = \delta(1-x) \frac{\left(G_E^2(Q^2) + \frac{Q^2}{4M^2} G_M^2(Q^2) \right)}{\left(1 + \frac{Q^2}{4M^2} \right)}, \quad (6)$$

with G_E^2 (G_M^2) being the proton electric (magnetic) elastic form factor.
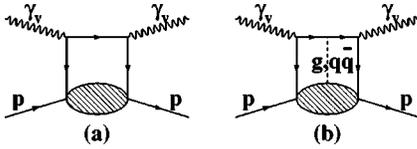
FIG. 2. Twist diagrams: (a) the leading twist contribution evaluated at leading order of PQCD, (b) the contribution of higher twists, where current quark and nucleon remnant can exchange by a system of particles consisting of gluons and $q\bar{q}$ pairs whose complexity is increasing with twist order.

For the leading $\tau = 2$ twist, one ends up in leading order (LO) or next-to-leading order (NLO) with the well-known perturbative logarithmic Q^2 evolution of singlet and non-singlet F_2 moments. However, if one wants to extend the analysis to small Q^2 and large x where the rest of the perturbative series becomes significant, some procedure for the summation of the higher orders of the PQCD expansion, such as the infrared renormalon model [13,14] or the recently developed soft-gluon resummation technique [15,16], has to be applied. For higher twists, $\tau > 2$, the power terms $E_{n\tau}(\mu)$ are related to quark-quark and quark-gluon correlations, as illustrated by Fig. 2, and should become important at small Q^2.

The systematic analysis of the Q^2 dependence of the experimentally derived Nachtmann moments $M_n^N(Q^2)$ in the intermediate Q^2 range $[0.5 < Q^2 < 10 \ (\text{GeV}/c)^2]$ should allow a separation of the higher twists from the leading twist. A precise evaluation would permit a comparison with the QCD predictions obtained from lattice simulations or a comparison with those models that describe the non-perturbative domain.

III. DATA ANALYSIS

The data were collected at TJNAF in Hall B with the CLAS detector and a liquid hydrogen target with thickness $\rho x = 0.35 \ \text{g/cm}^2$ during the electron beam running period in February–March 1999. The average beam current of 4.5 nA corresponded to a luminosity of $6 \times 10^{33} \ \text{cm}^{-2} \ \text{s}^{-1}$. To cover the largest interval in Q^2 and x, data were taken at five different electron beam energies: $E_0 = 1.5$, 2.5, 4.0, 4.2 and 4.4 GeV. The CLAS detector is a magnetic spectrometer based on a six-coil torus magnet whose field is primarily oriented along the azimuthal direction. The sectors, located between the magnet coils, are instrumented individually to form six essentially independent magnetic spectrometers. The particle detection system includes drift chambers (DC) for track reconstruction [17], scintillation counters (TOF) for the time of flight measurement [18], Cherenkov counters (CC) for electron identification [19], and electromagnetic calorimeters (EC) to measure neutrals and to improve the electron-pion separation [20]. The EC detectors have a granularity defined by triangular cells in the plane perpendicular to the incoming particles to study the electromagnetic shower shape and are longitudinally divided into two parts with the inner part acting as a pre-shower. Charged particles can be detected and identified for momenta down to 0.2 GeV/c and for polar angles between 8° and 142°. The CLAS superconducting coils reduce the acceptance of about 80% at $\theta = 90°$ to about 50% at forward angles ($\theta = 20°$), while the total acceptance for electrons is about 1.5 sr. Electron momentum resolution is a function of the scattered electron angle and it varies from 0.5% for $\theta \leq 30°$ up to 1%–2% for $\theta > 30°$. The angular resolution is approximately constant and approaching 1 mrad for polar and 4 mrad for azimuthal angles: the resolution on the momentum transfer ranges therefore from 0.2% up to 0.5%. The missing mass resolution was estimated 2.5 MeV for beam energy less than 3 GeV and about 7 MeV for larger energies. To study all possible multi-particle production, the acquisition trigger was configured to require at least one electron candidate in any of the sectors, where an electron candidate was defined as the coincidence of a signal in the EC and Cherenkov modules for each sector separately.

The accumulated statistics at the five energies is large enough ($> 6 \times 10^8$ triggers) to allow the extraction of the inclusive cross section with a rather small statistical error ($\leq 5\%$), in small x and Q^2 bins ($\Delta x = 0.009$, $\Delta Q^2 = 0.05 \ \text{GeV}^2$). The determination of the systematic error was more critical. CLAS is a large acceptance spectrometer and the response depends on the energy E' and the angle θ of the scattered electron. Determining the systematic effects of these, and other experimental parameters, is both necessary and complex. Consequently, we dedicate the next subsections to the discussion of the analysis procedure.

A. Momentum correction

Determining the momentum of a charged particle measured with CLAS depends on a proper understanding of the magnetic field geometry. As a result of the complexity of the detector and particularly the torus magnet system, it is crucial to check the reliability of the momentum determined by the DC tracking system. For this reason the position of the elastic peak was extracted from the measured inclusive electron cross section and compared to the theoretical value. A correction to the scattered electron momentum was applied to shift the elastic peak to the accepted value. The momentum correction obtained was small (from 2 to 7 MeV in W, depending on the beam energy) and resulted in significant improvement in the width of elastic peak .

The systematic error on the correction was estimated by comparing the position of the well-known second resonance peak [$S_{11}(1535)$ and $D_{13}(1520)$ resonances] to the position given in Refs. [21,22]. The position difference ΔW affects the cross section evaluation. The relative systematic error on the momentum correction is therefore given by

$$\delta_{mom}(x,Q^2) = \frac{\left| \sigma^B\left(W - \frac{\Delta W}{2}, Q^2\right) - \sigma^B\left(W + \frac{\Delta W}{2}, Q^2\right) \right|}{\sigma^B(W,Q^2)},$$

(7)

where σ^B represents the Bodek fit according to the parametrization from Refs. [21,22]. The systematic error calculated with Eq. (7) is given in Table I.

TABLE I. Range and average of systematic errors in F_2.

Source of uncertainties	Variation range [%]	Average [%]
Efficiency evaluation	1–9	4.3
e^+e^- pair production correction	0–3	0.3
Photoelectron correction	0.1–2.2	0.6
Radiative correction	1.5–20	3.2
Momentum correction	0.1–30	3.5
Uncertainty of $R = \sigma_L/\sigma_T$	0.5–5	2.4
Total	2.5–30	7.7

B. Electron identification and pion rejection

The electrons were identified by a combined off-line analysis of the signals from the four detector systems (DC, TOF, CC and EC). Only those electron candidates that were detected inside the most uniform ("fiducial") detector volume were analyzed. The electron yield was corrected separately in each kinematic bin for pion contamination, detection efficiency and radiative corrections.

The photoelectron distribution in the CC depends on the kinematics, and the contaminating pion peak can be completely removed only with large efficiency losses of about 30% in several kinematic regions. Therefore the pion contamination was removed by a two-step procedure. Electrons producing a large number of photoelectrons (see Fig. 4) were identified by an energy cut in the EC detector response. The pion contamination to electrons producing a small number of photoelectrons was removed by analysis of the CC response.

As an example of the first step, Fig. 3 shows the CC photoelectron distribution N_{phe} as a function of the fraction of energy deposited in the EC detector EC_{tot}/P for negatively charged particles emitted at $\theta < 35°$, momentum $P < 1$ GeV/c, and a beam energy of 2.5 GeV. The regions corresponding to pions ($N_{phe} \lesssim 2.5$) and to electrons ($EC_{tot}/P \gtrsim 0.25$) cannot be clearly separated and only the pion contamination to the left of the solid line can be removed without affecting the electron detection efficiency. The remaining pion contamination and the correction of the Cherenkov efficiency for electrons F_{phe} have determined by a combined fit of the measured photoelectron distribution with two Poisson distributions convoluted with a Gaussian function to account for the finite photomultiplier resolution as shown in Fig. 4.

The fit was performed separately for each sector over the whole kinematics data set ($\theta = 20° - 50°$ and $W = 0.9–2.5$ GeV).

To minimize the errors, the fit was performed in rather large bins ($\Delta\theta = 2°$ and $\Delta E' \sim 0.1$ GeV). Therefore, in order to apply the correction to the measured cross section, which was obtained with smaller bins, values of the correction were parametrized with the polynomial function

$$F_{phe}(\nu,\theta) = 1 + A(\nu - \nu_0) + (B + C\theta)(\nu - \nu_0)^2, \quad (8)$$

where A, B, C and ν_0 are free parameters and $\nu = E_0 - E'$ the electron energy transfer. The related systematic error δ_{phe}
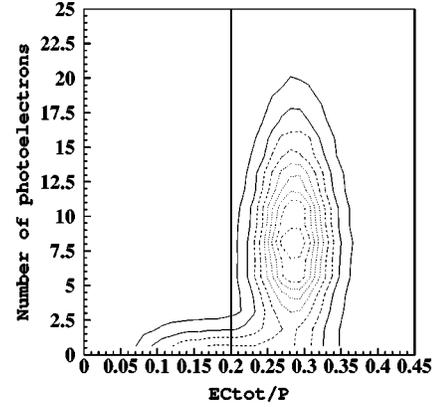
FIG. 3. Photoelectron distribution in the Cherenkov detector versus the energy deposited in the EC detector divided by the momentum of the particle as determined by the drift chamber. The black vertical line represents the cut to reduce the pion contamination.

$= \delta F_{phe}/F_{phe}$ is mainly due to the low statistics in those bins corresponding to large Q^2 values and was found to be less than 2%.

C. Background subtraction

Since the pair production background has not been measured, its contribution was estimated according to a model [23] based on the Wiser fit [24] of the inclusive pion photoproduction reaction. The most important source of e^+e^- pairs in the CLAS is due to π^0 production, which either decays to γe^+e^- (Dalitz decay) or to $\gamma\gamma$, with subsequent photon conversion to e^+e^-. The model was carefully checked, and it was in good agreement with the measured positron cross sections [23]; the difference was always less than 30%. The value of the correction was assumed to be
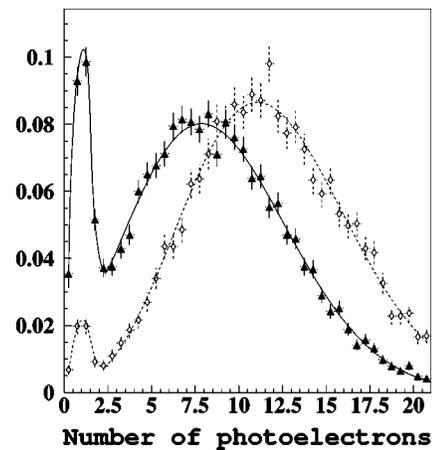
FIG. 4. The fitted photoelectron distribution for two different sets of kinematics after removing some of the pion contamination via the EC_{tot}/P cut: solid triangles show the distribution obtained with 4 GeV beam, scattered electron angle $\theta = 31°$ and momentum $P = 1$ GeV; open diamonds represent data taken with 2.5 GeV beam, scattered electron angle $\theta = 41°$ and momentum $P = 1$ GeV.

equal to the ratio of the inclusive e^+ production cross section σ_{e^+} over Bodek's fit [21,22] including radiative processes (tail from the elastic peak, bremsstrahlung, and Schwinger correction) σ_{rad}^B:

$$F_{e^+e^-}(E_0, E', \theta) = \frac{1}{1 + \dfrac{\sigma_{e^+}(E_0, E', \theta)}{\sigma_{rad}^B(E_0, E', \theta)}}. \quad (9)$$

The correction is generally small as expected in Ref. [7]; therefore, it was applied only for $E_0 > 2.0$ GeV and $W > 1.7$ GeV, where it was about 2%. The relative systematic error $\delta_{e^+e^-} = \delta F_{e^+e^-}/F_{e^+e^-}$ from this correction was estimated using uncertainties on σ_{e^+} given in Ref. [23].

In order to remove the contribution of scattering on the target walls, the empty target data were analyzed in the same way and subtracted from the inclusive data, after proper normalization. An additional source of background originating from knock-on electrons produced in the supporting structure of the detector was estimated and it found to be smaller than 0.3%.

D. Simulations

As a result of the complexity of the CLAS detector, the only way to study its response functions is to perform complete computer simulations, describing each subsystem in detail including all materials that make up each detector. The simulations of detector response to the scattered electron were performed according to the following procedure:

(i) Electron scattering events were generated by a random event generator with the probability distributed according to σ_{rad}^B, described above. The values of elastic and inelastic cross sections of the electron-proton scattering were taken from existing fits of world data, in Refs. [8] and [21,22], respectively. The internal radiative processes contribution was added according to calculations [25].

(ii) The generated events were passed through the standard CLAS GEANT-based simulation program [26], to model the detector response.

(iii) The results of the previous stage were further processed to make the detector response more realistic by adding the effects of electronic noise, background, dead wires and scintillator paddles.

(iv) Finally, the efficiency was calculated in each kinematic bin as a ratio of the number of reconstructed events, N_{rec}, over the number of generated events, N_{gen}:

$$\epsilon_{eff}(E_0, x, Q^2) = \frac{N_{rec}(E_0, x, Q^2)}{N_{gen}(E_0, x, Q^2)}. \quad (10)$$

The electron detection efficiency obtained from simulations is about 97% and approximately constant inside the fiducial region of the detector over the whole available kinematics.

In order to test the reliability of the simulation procedure and to check a proper absolute normalization, the well-
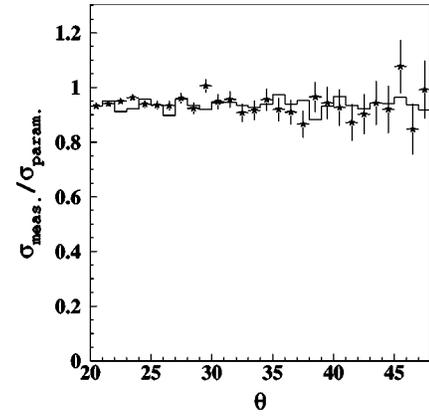
FIG. 5. Typical ratio of the measured elastic scattering cross section to the parametrization from Refs. [8,9] (points) with radiative corrections, in comparison to that obtained from the simulations (solid line); errors are statistical only.

known elastic scattering cross section was extracted from the same data set ($d\sigma/d\Omega_{expt}$) and compared to the simulated cross section ($d\sigma/d\Omega_{sim}$). The two cross sections are in good agreement within statistical and systematic errors as shown in Fig. 5.

The relative systematic deviation of the elastic cross section obtained from simulations and from these data δ_{eff}, was calculated for each beam energy and scattered electron angle (in bins of 1° on the accessible interval from 20° to 50°) according to:

$$\delta_{eff}^2(E_0, \theta) + \delta_{expt}^2(E_0, \theta)$$
$$= \left[\frac{\dfrac{d\sigma}{d\Omega}expt(E_0, \theta) - \dfrac{d\sigma}{d\Omega}sim(E_0, \theta)}{\dfrac{d\sigma}{d\Omega}fit(E_0, \theta)} \right]^2, \quad (11)$$

where $d\sigma/d\Omega_{fit}$ is the parametrization described in Ref. [8] and δ_{expt} is the statistical error of the measured elastic cross section. For the error propagation δ_{eff} was parametrized by a linear function of the scattered electron angle θ.

E. Inclusive inelastic cross section

Since the Monte Carlo simulations were shown to be reliable, they were used to evaluate efficiency, acceptance, bin centering and radiative corrections. For each kinematic bin, the inclusive cross section $d\sigma$ and the structure function F_2 were extracted directly from the raw electron yield N_{expt} normalized to the integrated luminosity and corrected for efficiency, acceptance, bin centering, and radiative effects as follows:

$$\frac{d^2\sigma}{dxdQ^2} = \frac{1}{\rho\frac{N_A}{M_A}LQ_{tot}}\frac{N_{expt}(x,Q^2)}{\epsilon(x,Q^2)}$$

$$\times F_{phe}(x,Q^2)F_{e^+e^-}(x,Q^2), \qquad (12)$$

where ρ is the density of liquid H_2 in the target, N_A is the Avogadro constant, M_A is the target molar mass, L is the target length, Q_{tot} is the total charge in the Faraday cup (FC) and $\epsilon(x,Q^2)$ is the efficiency defined in Eq. (10) with the radiative and bin-centering correction factors according to

$$\epsilon(x,Q^2) = \epsilon_{eff}(x,Q^2)\epsilon_{rad}(x,Q^2)\epsilon_{bin}(x,Q^2), \qquad (13)$$

where

$$\epsilon_{rad} = \frac{\sigma_{rad}^B}{\sigma^B} \quad \text{and} \quad \epsilon_{bin} = \frac{\int_{\Delta\tau}d\sigma^B}{\sigma^B}, \qquad (14)$$

and the integral was taken over the current bin area $\Delta\tau$. The radiative correction factor ϵ_{rad} strongly varies in the explored kinematic range from 0.85 up to 1.6. Fortunately, the largest correction was contributed by the elastic peak tail for which calculations are very accurate (see Refs. [25,27]).

All systematic uncertainties were propagated in quadrature to the final relative systematic error:

$$\delta_{sys}(x,Q^2) = [\delta_{eff}^2(x,Q^2) + \delta_{phe}^2(x,Q^2) + \delta_{e^+e^-}^2(x,Q^2)$$
$$+ \delta_{mom}^2(x,Q^2) + \delta_{rad}^2(x,Q^2)]^{1/2}, \qquad (15)$$

where δ_{rad} is the systematic uncertainty on the radiative correction, given by

$$\delta_{rad}(E,x,Q^2) = |\epsilon_{rad}^{TSAI}(E,x,Q^2) - \epsilon_{rad}^{POLRAD}(E,x,Q^2)|, \qquad (16)$$

where $\epsilon_{rad}^{TSAI}(E,x,Q^2)$ and $\epsilon_{rad}^{POLRAD}(E,x,Q^2)$ are the radiative correction factors in σ_{rad}^B evaluated with two different approaches ([25] and [27]). These two approaches use different parametrizations of the elastic ([8] and [28]) and inelastic ([21,22] and [29]) cross sections as well as different calculation techniques.

$\delta_{rad}(E,x,Q^2)$ varies in the kinematic range of the experiment from 0 to 20% while the average value is 3%. A minimum radiative correction systematic error of 1.5% was assumed.

F. Structure function $F_2(x,Q^2)$

The structure function $F_2(x,Q^2)$ was extracted from the inelastic cross section using the fit of the function $R(x,Q^2) \equiv \sigma_L/\sigma_T$ developed in [14] and described in Appendix A. The inclusive electron scattering cross section can be expressed in terms of the well known structure functions W_1 and W_2 as [12]

$$\frac{d^2\sigma}{d\Omega dE'} = \sigma_{Mott}\left\{2W_1(x,Q^2)\tan^2\frac{\theta}{2} + W_2(x,Q^2)\right\}, \qquad (17)$$

where the Mott cross section is given by

$$\sigma_{Mott} = \frac{\alpha^2\cos^2\frac{\theta}{2}}{4E^2\sin^4\frac{\theta}{2}}. \qquad (18)$$

Therefore, the structure function $F_2 = \nu W_2$ can be evaluated as follows:

$$F_2(x,Q^2) = \frac{1}{\sigma_{Mott}}\frac{d^2\sigma}{dxdQ^2}J\frac{\nu}{1+\frac{1-\epsilon}{\epsilon}\frac{1}{1+R}}, \qquad (19)$$

where J is the Jacobian given by

$$J = \frac{x(s-M^2)}{2\pi M\nu}E', \qquad (20)$$

where s is the squared invariant mass of the initial electron-proton system $s = M^2 + 2EM$ and ϵ is the polarization parameter defined as

$$\epsilon \equiv \left(1 + 2\frac{\nu^2+Q^2}{Q^2}\tan^2\frac{\theta}{2}\right)^{-1}. \qquad (21)$$

The function $R(x,Q^2)$ is poorly known in the resonance region; however, the structure function F_2 in the relevant kinematic range is very insensitive to the value of R. In fact even a 100% systematic uncertainty on R gives only a few percent uncertainty on F_2. The relative total systematic error is given by

$$\delta_{F_2}^{sys}(x,Q^2) = \left[\delta_{sys}^2(x,Q^2) + \left(\frac{1-\epsilon}{1+\epsilon R}\frac{\delta_R}{1+R}\right)^2\right]^{1/2}. \qquad (22)$$

The uncertainties of R given in Ref. [14] were propagated to the resulting F_2, and the actual systematic errors introduced by δ_R were always lower than 3%.

The combined statistical and systematic precision of the obtained structure function F_2 is strongly dependent on kinematics and the statistical errors vary from 0.2% up to 30% at the largest Q^2 where statistics are very limited. Figure 6 shows a comparison between the F_2 data from CLAS and the other world data in the $Q^2 = 0.775$ GeV^2 bin. The observed discrepancies with the data from Ref. [7] which fill the large x region in Fig. 6 are mostly within the systematic errors. Because of the much smaller bin centering corrections in this Q^2 region, our data are in a better agreement with data previously measured at SLAC, given in Ref. [22], and the parametrization of those from Refs. [21,22]. The average statistical uncertainty is about 5%; the systematic uncertainties range from 2.5% up to 30%, with the mean value estimated as 7.7% (see Table I). The values of $F_2(x,Q^2)$ determined using our data are tabulated elsewhere [10].
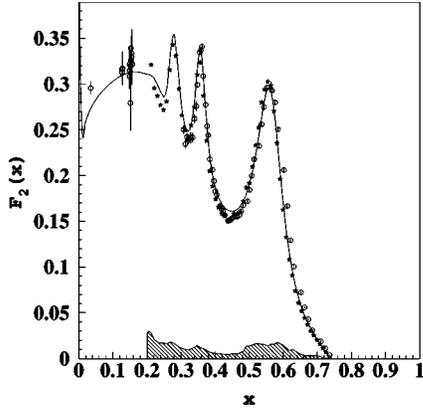
FIG. 6. Structure function $F_2(x,Q^2)$ at $Q^2=0.775$ GeV^2: stars represent experimental data obtained in the present analysis with systematic errors indicated by the hatched area, open circles show data from previous experiments [7,30–44] and the solid line represents the parametrization from Ref. [14].

G. Moments of the structure function F_2

As discussed in the Introduction, the final goal of this analysis is the evaluation of the Nachtmann moments of the structure function F_2. The total Nachtmann moments were computed as the sum of the elastic and inelastic moments:

$$M_n = M_n^{el} + M_n^{in}. \tag{23}$$

The contribution originating from the elastic peak was calculated according to the following expression from Ref. [14]:

$$M_n^{el} = \left(\frac{2}{1+r}\right)^{n+1} \frac{3+3(n+1)r+n(n+2)r^2}{(n+2)(n+3)}$$

$$\times \frac{G_E^2(Q^2)+\dfrac{Q^2}{4M^2}G_M^2(Q^2)}{1+\dfrac{Q^2}{4M^2}}, \tag{24}$$

where the proton form factors $G_E^2(Q^2)$ and $G_M^2(Q^2)$ are from Ref. [8] modified according the recently measured data on G_E/G_M [9], as described in Ref. [10].

The evaluation of the inelastic moment M_n^{in} involves the computation at fixed Q^2 of an integral over x. For this purpose, in addition to the results obtained from the CLAS data, world data on the structure function F_2 from Refs. [7,30–44] and data on the inelastic cross section [21,22,45] were used to reach an adequate coverage (see Fig. 1). The integral over x was performed numerically using the standard trapezoidal method TRAPER [46]. Data from Ref. [47] were not included in the analysis due to their inconsistency with other data sets as explained in detail in Ref. [48], and data from Refs. [49] and [50] were not included due to the large experimental uncertainties.

The Q^2 range from 0.05 to 3.75 (GeV/c)^2 was divided into $\Delta Q^2=0.05$ (GeV/c)^2 bins. Then within each Q^2 bin the world data were shifted to the central bin value Q_0^2, using the

fit of $F_2^B(x,Q^2)$ from Ref. [14]. Here the fit $F_2^B(x,Q^2)$ consists of two parts, a parametrization [21,22] in the resonance region ($W<2.5$ GeV), and a QCD-like fit from Ref. [51] in the DIS ($W>2.5$ GeV):

$$F_2(x,Q_0^2) = \frac{F_2(x,Q^2)}{F_2^B(x,Q^2)} F_2^B(x,Q_0^2). \tag{25}$$

The difference between the real and bin-centered data,

$$\delta_{F_2}^{cent}(x,Q^2) = F_2(x,Q^2)\left|1 - \frac{F_2^B(x,Q_0^2)}{F_2^B(x,Q^2)}\right|, \tag{26}$$

was added to the systematic errors of F_2 in extracting the Nachtmann moments. As an example, Fig. 7 shows the integrands of the first four moments as a function of x at fixed Q^2. The significance of the large x region for various moments can clearly be seen.

To have a data set dense in x, which reduces the error in the numerical integration, we performed an interpolation, at each fixed Q_0^2, when two contiguous experimental data points differed by more than ∇. The value of ∇ depended on kinematics; in the resonance region where the structure function exhibits strong variations, ∇ had to be smaller than half the resonance widths and was parametrized as $\nabla = 0.04/[1+\sqrt{Q^2/10}]$. Above the resonances, where F_2 is smooth, we only accounted for the fact that the available x region decreases with decreasing Q^2 ($\nabla = 0.1[1+\sqrt{Q^2/10}]$). Finally in the low x region ($x<0.03$) where the F_2 shape depends weakly on Q^2, but strongly on x, we set $\nabla = 0.015$. Changing these ∇ values by as much as a factor of 2 produced changes in the moments that were much smaller than the systematic errors.

To fill the gap within two contiguous points x_a and x_b, we used the interpolation function $F_2^{int}(x,Q_0^2)$ defined as the parametrization from Ref. [14] normalized to the experimental data on both edges of the interpolating range. Assuming that the shape of the fit is correct,

$$F_2^{int}(x,Q_0^2) = \alpha(Q_0^2)F_2^B(x,Q_0^2), \tag{27}$$

where the normalization factor $\alpha(Q_0^2)$ is defined as the weighted average, evaluated using all experimental points located within an interval Δ around x_a or x_b:

$$\alpha(Q_0^2) = \delta_N^2(Q_0^2)\left[\sum_i^{|x_i-x_a|<\Delta} \frac{F_2(x_i,Q_0^2)/F_2^B(x_i,Q_0^2)}{(\delta_{F_2}^{stat}(x_i,Q_0^2))^2} \right.$$
$$\left. + \sum_j^{|x_j-x_b|<\Delta} \frac{F_2(x_j,Q_0^2)/F_2^B(x_j,Q_0^2)}{(\delta_{F_2}^{stat}(x_j,Q_0^2))^2}\right], \tag{28}$$

where $\delta_{F_2}^{stat}(x_j,Q_0^2)$ is the statistical error relative to F_2^B and
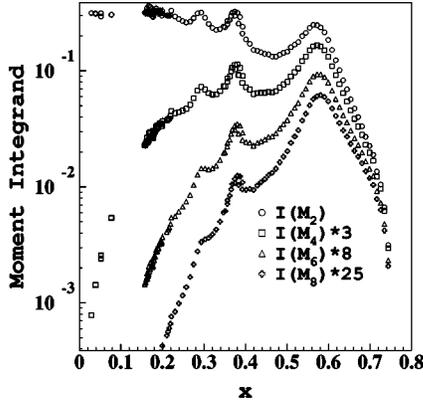
FIG. 7. Integrands of the inelastic Nachtmann moments at $Q^2 = 0.825$ GeV^2: circles represent the integrand of the M_2, squares show the integrand of the M_4, triangles represent the integrand of the M_6 and crosses represent the integrand of the M_8.

$$\delta_N(Q_0^2) = \left[\sum_i^{|x_i - x_a| < \Delta} \frac{1}{(\delta_{F_2}^{stat}(x_i, Q_0^2))^2} + \sum_j^{|x_j - x_b| < \Delta} \frac{1}{(\delta_{F_2}^{stat}(x_j, Q_0^2))^2} \right]^{-1/2} \quad (29)$$

is the statistical uncertainty of the normalization. Therefore, the statistical error of the moments calculated according the trapezoidal rule [46] was increased by adding the linearly correlated contribution from each interpolation interval as follows:

$$\delta_n^{norm}(Q_0^2) = \delta_N(Q_0^2) \int_{x_a}^{x_b} dx \frac{\xi^{n+1}}{x^3} F_2^B(x, Q_0^2)$$

$$\times \frac{3 + 3(n+1)r + n(n+2)r^2}{(n+2)(n+3)}. \quad (30)$$

Since we average the ratio $F_2(x_i, Q_0^2)/F_2^B(x_i, Q_0^2)$, Δ is not affected by the resonance structures, and its value was fixed to have more than two experimental points in most cases; therefore, Δ was chosen equal to 0.03 in the resonance and in the very low x regions and to 0.05 in the DIS region. In Fig. 8 we show how this interpolation is applied: the thin solid line represents the original function $F_2^B(x, Q^2)$ and the heavy solid line represents the result of the interpolation $F_2^{int}(x, Q^2)$. We also checked that the moments do not show any dependence on the Δ values.

To fill the gap between the last experimental point and one of the integration limits ($x_a = 0$ or $x_b = 1$) we performed an extrapolation at each fixed Q_0^2 using $F_2^B(x, Q_0^2)$ including its systematic error given in Ref. [14].

As an extension of the analysis, the world data at Q^2 above 5 $(\text{GeV}/c)^2$ were analyzed in the same way as described above. The only differences were the Q^2 bin size, which was chosen equal to 5% of Q^2, and the values of the parameters ∇ and Δ. In addition, the bins were situated not continuously, but only where data exist. Since at large Q^2 the
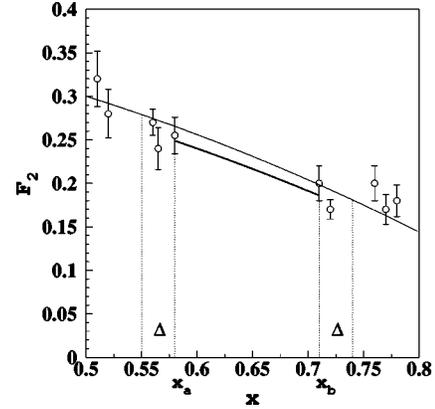
FIG. 8. Example of the interpolating procedure. The meaning of the curves and symbols is described in the text.

shape of $F_2(x)$ remains almost constant with changing Q^2, both parameters ∇ and Δ were fixed: in the resonance region ($W < 1.8$ GeV) to value 0.01; 0.1 in the DIS; and $\nabla = 0.005$ and $\Delta = 0.01$ at very low x ($x < 0.03$). The results for $M_n^{in}(Q^2)$ did not exhibit any significant dependence on the choice of the parameter values. The results are reported together with their statistical and systematic errors in Table II.

H. Systematic errors of the moments

The systematic error consists of genuine uncertainties in the data given in Refs. [7,21,22,30–45] and uncertainties in the evaluation procedure. To estimate the first type of error we had to account for using many data sets measured in different laboratories and with different detectors. In the present analysis we assume that different experiments are independent and therefore only systematic errors within one data set are correlated.

Thus, an upper limit for the contribution of the systematic error from each data set was evaluated in the following way:

(i) we first applied a simultaneous shift to all experimental points in this set by an amount equal to their systematic error;

(ii) then the inelastic nth moments obtained using these distorted data $\tilde{M}_{n(i)}^{in}(Q^2)$ were compared to the original moments $M_n^{in}(Q^2)$ evaluated with no systematic shifts;

(iii) finally the deviations for each data set were summed in quadrature as independent values:

$$\delta_n^D(Q^2) = \frac{1}{M_n^{in}(Q^2)} \sqrt{\sum_i^{N_S} [\tilde{M}_{n(i)}^{in}(Q^2) - M_n^{in}(Q^2)]^2}, \quad (31)$$

where N_S is the number of available data sets. The resulting error was summed in quadrature to $\delta_n^{norm}(Q^2)$ to finally evaluate the total systematic error of the nth moment.

The second type of error is related to the bin centering, interpolation and extrapolation. The bin centering systematic uncertainty was estimated as follows:

$$\delta_n^C(Q^2) = \sum_i K_n(x_i, Q^2) w_i(Q^2) \delta_{F_2}^{cent}(x_i, Q^2), \quad (32)$$

TABLE II. The inelastic Nachtmann moments for $n = 2,4,6$ and 8 evaluated in the interval $0.05 \leq Q^2 \leq 100$ $(\text{GeV}/c)^2$. The moments are labeled with $*$ when the contribution to the integral by the experimental data is between 50% and 70%; all other values were evaluated with more than 70% data coverage. The data are reported together with the statistical and systematic errors.

Q^2 [$(\text{GeV}/c)^2$]	$M_2(Q^2) \times 10^{-1}$	$M_4(Q^2) \times 10^{-2}$	$M_6(Q^2) \times 10^{-3}$	$M_8(Q^2) \times 10^{-3}$
0.075	$0.202 \pm 0.002 \pm 0.009$	$0.016 \pm 0.0005 \pm 0.001$	$0.0019 \pm 0.0001 \pm 0.0001$	
0.125	$0.451 \pm 0.006 \pm 0.025$	$0.072 \pm 0.002 \pm 0.004$	$0.017 \pm 0.001 \pm 0.001$	
0.175	$0.638 \pm 0.005 \pm 0.025$	$0.162 \pm 0.002 \pm 0.007$	$0.060 \pm 0.001 \pm 0.003$	$0.0025 \pm 0.0001 \pm 0.0001$
0.225	$0.775 \pm 0.003 \pm 0.026$	$0.248 \pm 0.001 \pm 0.008$	$0.119 \pm 0.001 \pm 0.004$	$0.0064 \pm 0.0001 \pm 0.0002$
0.275	$0.910 \pm 0.004 \pm 0.030$	$0.364 \pm 0.002 \pm 0.015$	$0.218 \pm 0.002 \pm 0.010$	$0.0146 \pm 0.0001 \pm 0.0007$
0.325	$1.000 \pm 0.002 \pm 0.040$	$0.465 \pm 0.0005 \pm 0.026$	$0.328 \pm 0.0005 \pm 0.020$	$0.0259 \pm 0.00005 \pm 0.0017$
0.375	$1.114 \pm 0.002 \pm 0.047$	$0.587 \pm 0.0005 \pm 0.033$	$0.478 \pm 0.0005 \pm 0.030$	$0.0439 \pm 0.00005 \pm 0.0029$
0.425	$1.209 \pm 0.005 \pm 0.037$	$0.704 \pm 0.001 \pm 0.034$	$0.644 \pm 0.001 \pm 0.038$	$0.0670 \pm 0.0001 \pm 0.0043$
0.475	$1.298 \pm 0.008 \pm 0.036$	$0.839 \pm 0.003 \pm 0.023$	$0.858 \pm 0.003 \pm 0.024$	$0.1002 \pm 0.0004 \pm 0.0030$
0.525	$1.347 \pm 0.004 \pm 0.047$	$0.916 \pm 0.003 \pm 0.038$	$1.010 \pm 0.005 \pm 0.046$	$0.1279 \pm 0.0008 \pm 0.0062$
0.575	$1.419 \pm 0.003 \pm 0.049$	$1.023 \pm 0.002 \pm 0.050$	$1.215 \pm 0.002 \pm 0.068$	$0.1660 \pm 0.0003 \pm 0.0101$
0.625	$1.444 \pm 0.006 \pm 0.059$	$1.110 \pm 0.003 \pm 0.041$	$1.413 \pm 0.005 \pm 0.057$	$0.2079 \pm 0.0009 \pm 0.0090$
0.675	$1.514 \pm 0.004 \pm 0.051$	$1.191 \pm 0.001 \pm 0.062$	$1.603 \pm 0.002 \pm 0.098$	$0.2507 \pm 0.0005 \pm 0.0168$
0.725	$1.554 \pm 0.006 \pm 0.050$	$1.267 \pm 0.001 \pm 0.059$	$1.785 \pm 0.002 \pm 0.102$	$0.2946 \pm 0.0004 \pm 0.0190$
0.775	$1.578 \pm 0.007 \pm 0.049$	$1.345 \pm 0.002 \pm 0.053$	$1.996 \pm 0.002 \pm 0.087$	$0.3484 \pm 0.0005 \pm 0.0160$
0.825	$1.606 \pm 0.006 \pm 0.050$	$1.389 \pm 0.002 \pm 0.066$	$2.130 \pm 0.003 \pm 0.117$	$0.3860 \pm 0.0006 \pm 0.0233$
0.875	$1.625 \pm 0.019 \pm 0.074$	$1.452 \pm 0.005 \pm 0.065$	$2.320 \pm 0.004 \pm 0.122$	$0.4393 \pm 0.0008 \pm 0.0254$
0.925	$1.649 \pm 0.014 \pm 0.040$	$1.500 \pm 0.005 \pm 0.058$	$2.476 \pm 0.005 \pm 0.119$	$0.4866 \pm 0.0010 \pm 0.0264$
0.975	$1.669 \pm 0.013 \pm 0.044$	$1.553 \pm 0.005 \pm 0.058$	$2.651 \pm 0.007 \pm 0.113$	$0.5416 \pm 0.0015 \pm 0.0254$
1.025	$1.673 \pm 0.011 \pm 0.049$	$1.584 \pm 0.004 \pm 0.061$	$2.785 \pm 0.011 \pm 0.116$	$0.5887 \pm 0.0030 \pm 0.0248$
1.075	$1.706 \pm 0.011 \pm 0.046$	$1.597 \pm 0.004 \pm 0.067$	$2.820 \pm 0.005 \pm 0.140$	$0.6048 \pm 0.0012 \pm 0.0322$
1.125		$1.648 \pm 0.003 \pm 0.076$	$3.002 \pm 0.005 \pm 0.150$	$0.6627 \pm 0.0013 \pm 0.0370$
1.175		$1.701 \pm 0.004 \pm 0.055$	$3.179 \pm 0.007 \pm 0.117$	$0.7236 \pm 0.0018 \pm 0.0298$
1.225	$1.722 \pm 0.009 \pm 0.045$	$1.706 \pm 0.005 \pm 0.066$	$3.245 \pm 0.009 \pm 0.154$	$0.7525 \pm 0.0020 \pm 0.0402$
1.275	$1.736 \pm 0.006 \pm 0.086$	$1.732 \pm 0.005 \pm 0.060$	$3.364 \pm 0.012 \pm 0.126$	$0.8021 \pm 0.0036 \pm 0.0309$
1.325	$1.792 \pm 0.015 \pm 0.050$	$1.828 \pm 0.004 \pm 0.076$	$3.561 \pm 0.011 \pm 0.178$	$0.8556 \pm 0.0033 \pm 0.0475$
1.375	$1.798 \pm 0.027 \pm 0.055$	$1.839 \pm 0.004 \pm 0.082$	$3.630 \pm 0.008 \pm 0.189$	$0.8864 \pm 0.0024 \pm 0.0516$
1.425	$1.815 \pm 0.007 \pm 0.049$	$1.873 \pm 0.004 \pm 0.073$	$3.741 \pm 0.011 \pm 0.173$	$0.9280 \pm 0.0032 \pm 0.0492$
1.475	$1.833 \pm 0.006 \pm 0.053$	$1.899 \pm 0.004 \pm 0.073$	$3.839 \pm 0.010 \pm 0.154$	$0.9669 \pm 0.0031 \pm 0.0397$
1.525	$1.844 \pm 0.008 \pm 0.055$	$1.931 \pm 0.004 \pm 0.082$	$3.968 \pm 0.012 \pm 0.187$	$1.0158 \pm 0.0042 \pm 0.0488$
1.575	$1.833 \pm 0.006 \pm 0.065$	$1.940 \pm 0.004 \pm 0.096$	$4.022 \pm 0.010 \pm 0.249$	$1.0395 \pm 0.0033 \pm 0.0725$
1.625	$1.862 \pm 0.020 \pm 0.053$	$1.953 \pm 0.005 \pm 0.091$	$4.116 \pm 0.010 \pm 0.252$	$1.0859 \pm 0.0034 \pm 0.0772$
1.675		$1.957 \pm 0.005 \pm 0.083$	$4.170 \pm 0.011 \pm 0.231$	$1.1173 \pm 0.0036 \pm 0.0740$
1.725	$1.857 \pm 0.023 \pm 0.049$	$1.998 \pm 0.005 \pm 0.075$	$4.316 \pm 0.013 \pm 0.218$	$1.1680 \pm 0.0043 \pm 0.0726$
1.775	$1.884 \pm 0.063 \pm 0.054$	$2.020 \pm 0.011 \pm 0.072$	$4.412 \pm 0.012 \pm 0.194$	$1.2081 \pm 0.0043 \pm 0.0628$
1.825	$1.862 \pm 0.010 \pm 0.053$	$2.024 \pm 0.006 \pm 0.072$	$4.459 \pm 0.015 \pm 0.168$	$1.2338 \pm 0.0050 \pm 0.0462$
1.875	$1.837 \pm 0.015 \pm 0.060$	$2.014 \pm 0.006 \pm 0.101$	$4.446 \pm 0.015 \pm 0.256$	$1.2363 \pm 0.0046 \pm 0.0798$
1.925		$2.026 \pm 0.006 \pm 0.093$	$4.551 \pm 0.015 \pm 0.243$	$1.2903 \pm 0.0047 \pm 0.0755$
1.975	$1.866 \pm 0.010 \pm 0.059$	$2.027 \pm 0.007 \pm 0.091$	$4.539 \pm 0.018 \pm 0.253$	$1.2857 \pm 0.0058 \pm 0.0824$
2.025	$1.831 \pm 0.014 \pm 0.046$	$2.037 \pm 0.007 \pm 0.092$	$4.677 \pm 0.020 \pm 0.263$	$1.3480 \pm 0.0069 \pm 0.0867$
2.075		$2.046 \pm 0.008 \pm 0.084$	$4.699 \pm 0.022 \pm 0.232$	$1.3694 \pm 0.0084 \pm 0.0750$
2.125	$1.870 \pm 0.022 \pm 0.052$	$2.074 \pm 0.008 \pm 0.092$	$4.825 \pm 0.022 \pm 0.269$	$1.4239 \pm 0.0082 \pm 0.0903$
2.175	$1.846 \pm 0.013 \pm 0.059$	$2.064 \pm 0.010 \pm 0.098$	$4.850 \pm 0.024 \pm 0.282$	$1.4421 \pm 0.0092 \pm 0.0945$
2.225		$2.053 \pm 0.012 \pm 0.089$	$4.825 \pm 0.024 \pm 0.267$	$1.4442 \pm 0.0093 \pm 0.0912$
2.275	$1.852 \pm 0.020 \pm 0.050$	$2.062 \pm 0.008 \pm 0.095$	$4.852 \pm 0.023 \pm 0.271$	$1.4606 \pm 0.0092 \pm 0.0917$
2.325	$1.859 \pm 0.012 \pm 0.058$	$2.081 \pm 0.009 \pm 0.108$	$4.984 \pm 0.025 \pm 0.291$	$1.5149 \pm 0.0098 \pm 0.0959$
2.375	$1.867 \pm 0.012 \pm 0.055$	$2.060 \pm 0.008 \pm 0.101$	$4.876 \pm 0.023 \pm 0.275$	$1.4832 \pm 0.0091 \pm 0.0921$
2.425		$2.051 \pm 0.008 \pm 0.107$	$4.860 \pm 0.023 \pm 0.257$	$1.4835 \pm 0.0089 \pm 0.0850$
2.475	$1.793 \pm 0.068 \pm 0.089$	$2.056 \pm 0.010 \pm 0.082$	$4.971 \pm 0.020 \pm 0.234$	$1.5362 \pm 0.0079 \pm 0.0796$
2.525	$1.845 \pm 0.031 \pm 0.066$	$2.035 \pm 0.010 \pm 0.110$	$4.899 \pm 0.018 \pm 0.260$	$1.5176 \pm 0.0063 \pm 0.0751$
2.575	$1.841 \pm 0.019 \pm 0.052$	$2.050 \pm 0.010 \pm 0.103$	$4.972 \pm 0.021 \pm 0.280$	$1.5556 \pm 0.0078 \pm 0.0915$
2.625		$2.035 \pm 0.011 \pm 0.122$	$4.884 \pm 0.024 \pm 0.293$	$1.5218 \pm 0.0087 \pm 0.0933$

TABLE II. (*Continued*).

$Q^2\ [(\mathrm{GeV}/c)^2]$	$M_2(Q^2)\times10^{-1}$	$M_4(Q^2)\times10^{-2}$	$M_6(Q^2)\times10^{-3}$	$M_8(Q^2)\times10^{-3}$
2.675		$2.018\pm0.009\pm0.024$	$4.896\pm0.022\pm0.277$	$1.5457\pm0.0091\pm0.0988$
2.725		$2.028\pm0.011\pm0.099$	$4.933\pm0.025\pm0.283$	$1.5634\pm0.0094\pm0.0970$
2.775		$2.028\pm0.017\pm0.107$	$4.931\pm0.029\pm0.293$	$1.5677\pm0.0096\pm0.0989$
2.825	$1.836\pm0.026\pm0.061$	$2.031\pm0.014\pm0.118$	$5.004\pm0.028\pm0.326$	$1.6030\pm0.0098\pm0.1081$
2.875	$1.839\pm0.016\pm0.057$	$2.019\pm0.013\pm0.108$	$4.976\pm0.027\pm0.309$	$1.6032\pm0.0098\pm0.1036$
2.925		$2.023\pm0.016\pm0.112$	$5.007\pm0.033\pm0.303$	$1.6219\pm0.0104\pm0.0970$
2.975	$1.843\pm0.033\pm0.050$	$2.018\pm0.014\pm0.102$	$4.983\pm0.027\pm0.294$	$1.6145\pm0.0092\pm0.0941$
3.025	$1.816\pm0.068\pm0.058$	$1.978\pm0.016\pm0.104$	$4.926\pm0.027\pm0.314$	$1.6042\pm0.0090\pm0.1057$
3.075	$1.804\pm0.060\pm0.055$	$1.992\pm0.022\pm0.114$	$4.942\pm0.040\pm0.352$	$1.6136\pm0.0119\pm0.1222$
3.125				$1.6293\pm0.0118\pm0.1491$
3.175		$2.011\pm0.031\pm0.141$	$5.002\pm0.064\pm0.372$	$1.6524\pm0.0159\pm0.1310$
3.225		$1.968\pm0.021\pm0.112$	$4.916\pm0.040\pm0.358$	$1.6289\pm0.0122\pm0.1315$
3.275		$2.007\pm0.022\pm0.116$	$4.985\pm0.043\pm0.351$	$1.6478\pm0.0127\pm0.1304$
3.325	$1.808\pm0.033\pm0.080$	$1.979\pm0.014\pm0.096$	$4.944\pm0.032\pm0.332$	$1.6321\pm0.0120\pm0.1264$
3.375	$1.804\pm0.029\pm0.055$	$1.981\pm0.016\pm0.086$	$4.976\pm0.031\pm0.312$	$1.6543\pm0.0119\pm0.1243$
3.425			$5.034\pm0.035\pm0.325$	$1.6787\pm0.0125\pm0.1285$
3.475		$1.943\pm0.013\pm0.064$	$4.915\pm0.032\pm0.253$	$1.6489\pm0.0118\pm0.1079$
3.525		$1.951\pm0.021\pm0.088$	$4.999\pm0.052\pm0.316$	$1.6918\pm0.0168\pm0.1238$
3.575			$5.021\pm0.043\pm0.268$	$1.6858\pm0.0142\pm0.1049$
3.625				
3.675		$1.930\pm0.024\pm0.040$	$4.857\pm0.063\pm0.310$	$1.6493\pm0.0197\pm0.1199$
3.725				$1.6698\pm0.0160\pm0.1276$
5.967		$1.810\pm0.015\pm0.116$	$4.597\pm0.044\pm0.553$	
7.268		$1.743\pm0.011\pm0.044$		
7.645			$4.374\pm0.044\pm0.098$	$1.5659\pm0.0202\pm0.0396$
8.027			$4.279\pm0.027\pm0.135$	$1.5205\pm0.0107\pm0.0642$
8.434		$1.653\pm0.014\pm0.084$	$4.223\pm0.032\pm0.109$	$1.5264\pm0.0122\pm0.0419$
8.857	$1.723\pm0.015\pm0.041$	$1.645\pm0.019\pm0.027$	$4.108\pm0.042\pm0.109$	$1.4712\pm0.0138\pm0.0566$
9.781		$1.653\pm0.010\pm0.061$	$4.130\pm0.034\pm0.146$	$1.4818\pm0.0167\pm0.0666$
10.267	$1.752\pm0.015\pm0.052$	$1.622\pm0.019\pm0.031$	$4.016\pm0.035\pm0.095$	$1.4321\pm0.0113\pm0.0367$
10.793			$3.987\pm0.106\pm0.761$	$1.4256\pm0.0175\pm0.1103$
11.345	$1.731\pm0.016\pm0.041$	$1.573\pm0.018\pm0.035$	$3.853\pm0.041\pm0.140$	$1.3644\pm0.0176\pm0.0793$
11.939	$1.759\pm0.008\pm0.042$	$1.596\pm0.013\pm0.031$	$3.910\pm0.040\pm0.111$	$1.3860\pm0.0181\pm0.0574$
13.185		$1.525\pm0.016\pm0.021$	$3.681\pm0.029\pm0.067$	$1.3011\pm0.0091\pm0.0336$
15.310	$1.686\pm0.014\pm0.074$	$1.471\pm0.019\pm0.032$	$3.533\pm0.044\pm0.133$	
16.902	$1.718\pm0.010\pm0.051$	$1.450\pm0.017\pm0.025$	$3.392\pm0.058\pm0.073$	$1.1752\pm0.0252\pm0.0283$
18.697	$1.679\pm0.033\pm0.097$	$1.401\pm0.013\pm0.027$	$3.275\pm0.039\pm0.088$	$1.1377\pm0.0147\pm0.0346$
19.629				$*1.1061\pm0.0221\pm0.0473$
21.625	$1.677\pm0.008\pm0.041$			
24.192	$*1.711\pm0.007\pm0.114$	$1.385\pm0.008\pm0.024$		$*1.0751\pm0.0143\pm0.0433$
26.599	$*1.665\pm0.062\pm0.135$			
28.192	$*1.702\pm0.009\pm0.140$	$1.344\pm0.007\pm0.037$		$*1.0109\pm0.0096\pm0.0808$
31.858	$*1.703\pm0.010\pm0.096$			
36.750	$*1.696\pm0.013\pm0.111$	$1.314\pm0.009\pm0.057$	$2.971\pm0.027\pm0.313$	$*1.0027\pm0.0135\pm0.1906$
44.000	$*1.681\pm0.013\pm0.085$			
49.750	$*1.658\pm0.019\pm0.101$			
57.000	$*1.694\pm0.017\pm0.170$			
64.884	$*1.636\pm0.043\pm0.114$	$1.222\pm0.053\pm0.044$	$2.708\pm0.082\pm0.193$	$*0.8945\pm0.0161\pm0.1164$
75.000		$*1.206\pm0.008\pm0.025$	$*2.651\pm0.024\pm0.150$	
88.000	$*1.669\pm0.088\pm0.075$	$*1.199\pm0.038\pm0.035$	$*2.630\pm0.057\pm0.202$	
99.000		$*1.179\pm0.012\pm0.034$	$*2.568\pm0.029\pm0.228$	
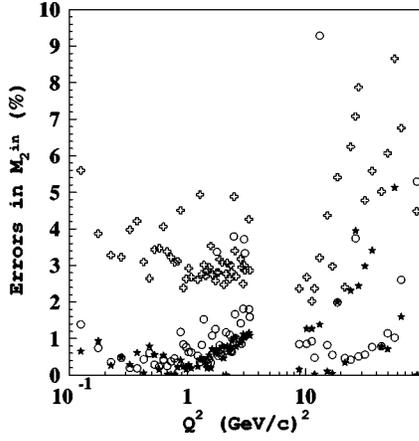
FIG. 9. Errors of the inelastic Nachtmann moment M_2 in percentage: open circles represent statistical errors, open crosses show the systematic error obtained in Eq. (36) and the difference between inelastic moments extracted using two different F_2 parametrizations [14] and [52] at $W > 2.5$ GeV is shown by stars.

where according the Nachtmann moment definition and the trapezoidal integration rule

$$K_n(x_i, Q^2) = \frac{\xi_i^{n+1}}{x_i^3} \frac{3 + 3(n+1)r_i + n(n+2)r_i^2}{(n+2)(n+3)},$$

$$w_i(Q^2) = (x_{i+1} - x_{i-1})/2. \tag{33}$$

The relative systematic error of the interpolation was estimated as the possible change of the fitting function slope in the interpolation interval, and it was evaluated as a difference in the normalization at different edges:

$$\delta_S(Q_0^2) = \left| \frac{1}{N_i} \sum_i^{|x_i - x_a| < \Delta} \frac{F_2(x_i, Q_0^2)}{F_2^B(x_i, Q_0^2)} - \frac{1}{N_j} \sum_j^{|x_j - x_b| < \Delta} \frac{F_2(x_j, Q_0^2)}{F_2^B(x_j, Q_0^2)} \right|, \tag{34}$$

where N_i and N_j are the number of points used to evaluate the sums. Since the structure function $F_2(x, Q^2)$ is a very smooth function of x below resonances, on the limited x interval (smaller than ∇) the linear approximation gives a good estimate. Thus, the error given in Eq. (34) accounts for such a linear mismatch between the fitting function and the data on the interpolation interval. Meanwhile, the CLAS data cover all the resonance region and no interpolation was used there. Therefore, the total systematic error introduced in the corresponding moment by the interpolation can be estimated as

$$\delta_n^I(Q_0^2) = \delta_S(Q_0^2) \int_{x_a}^{x_b} dx \frac{\xi^{n+1}}{x^3} F_2^B(x, Q_0^2)$$

$$\times \frac{3 + 3(n+1)r + n(n+2)r^2}{(n+2)(n+3)}. \tag{35}$$
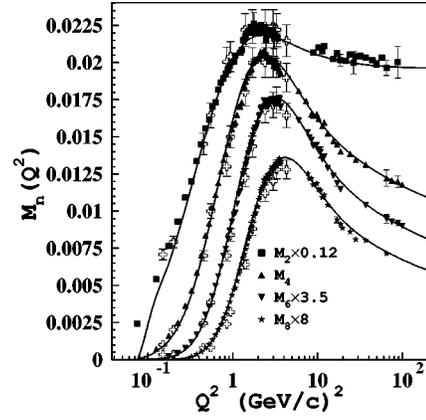
FIG. 10. The inelastic Nachtman moments extracted from the world data, including the new CLAS results, are shown as the solid shapes, while the solid line represents moments obtained in Ref. [14]. The open crosses indicate the Nachtman moments determined in Ref. [2]. Errors are statistical only.

The systematic errors obtained by these procedures were summed in quadrature:

$$\delta_n^P(Q^2) = \sqrt{[\delta_n^D(Q^2)]^2 + [\delta_n^C(Q^2)]^2 + [\delta_n^I(Q^2)]^2}. \tag{36}$$

In order to study the systematic error in the extrapolation at very low x we have performed a test of the functional form dependence comparing moments presented here with those obtained by using the fitting function from the neural network parametrization of Ref. [52]. The difference is significant only for M_2 and it appeared to be smaller than $\delta_n^P(Q^2)$ given by Eq. (36) (see Fig. 9). The difference was added to $\delta_n^P(Q^2)$ in quadrature to evaluate the total systematic error of the nth moment.

IV. EXTRACTION OF LEADING AND HIGHER TWISTS

In this section, we present our twist analysis of the moments we have extracted, which are presented in Fig. 10. As already shown in Refs. [14] and [16], the extraction of higher twists at large x depends significantly on the effects of PQCD high-order corrections. In particular, the use of the well established NLO approximation for the leading twist is known to lead to unreliable results for the higher twists [16]. Therefore, hereafter we follow Ref. [16], where the PQCD corrections beyond the NLO are estimated according to soft gluon resummation (SGR) techniques.

As far as power corrections are concerned, several higher-twist operators exist and mix under the renormalization-group equations. Such mixings are rather involved and the number of mixing operators increases with the order n of the moment. Since a complete calculation of the higher-twist anomalous dimensions is not yet available, we use the same phenomenological ansatz already adopted in Refs. [14] and [16]. Thus, our extracted Nachtmann moments are analyzed in terms of the twist expansion

$$M_n^N(Q^2) = \eta_n(Q^2) + HT_n(Q^2), \tag{37}$$

TABLE III. Extracted parameters of the twist expansion. The contribution of higher twists to M_2 was too small to be extracted by the present procedure.

	M_2	M_4	M_6	M_8
A_2	0.174 ± 0.006	$(1.61 \pm 0.04) \times 10^{-2}$	$(3.98 \pm 0.18) \times 10^{-3}$	$(1.39 \pm 0.07) \times 10^{-3}$
$a^{(4)}$	$(1.4 \pm 1.8) \times 10^{-3}$	$(3.6 \pm 1.4) \times 10^{-4}$	$(1.9 \pm 0.14) \times 10^{-4}$	$(1.69 \pm 0.16) \times 10^{-4}$
$\gamma^{(4)}$	-	5.7 ± 0.6	7.4 ± 0.3	6.2 ± 0.3
$a^{(6)}$	-	$(-9.5 \pm 3.4) \times 10^{-5}$	$(-6.57 \pm 0.53) \times 10^{-5}$	$(-5.75 \pm 0.44) \times 10^{-5}$
$\gamma^{(6)}$	-	4.4 ± 0.6	5.7 ± 0.3	4.6 ± 0.3
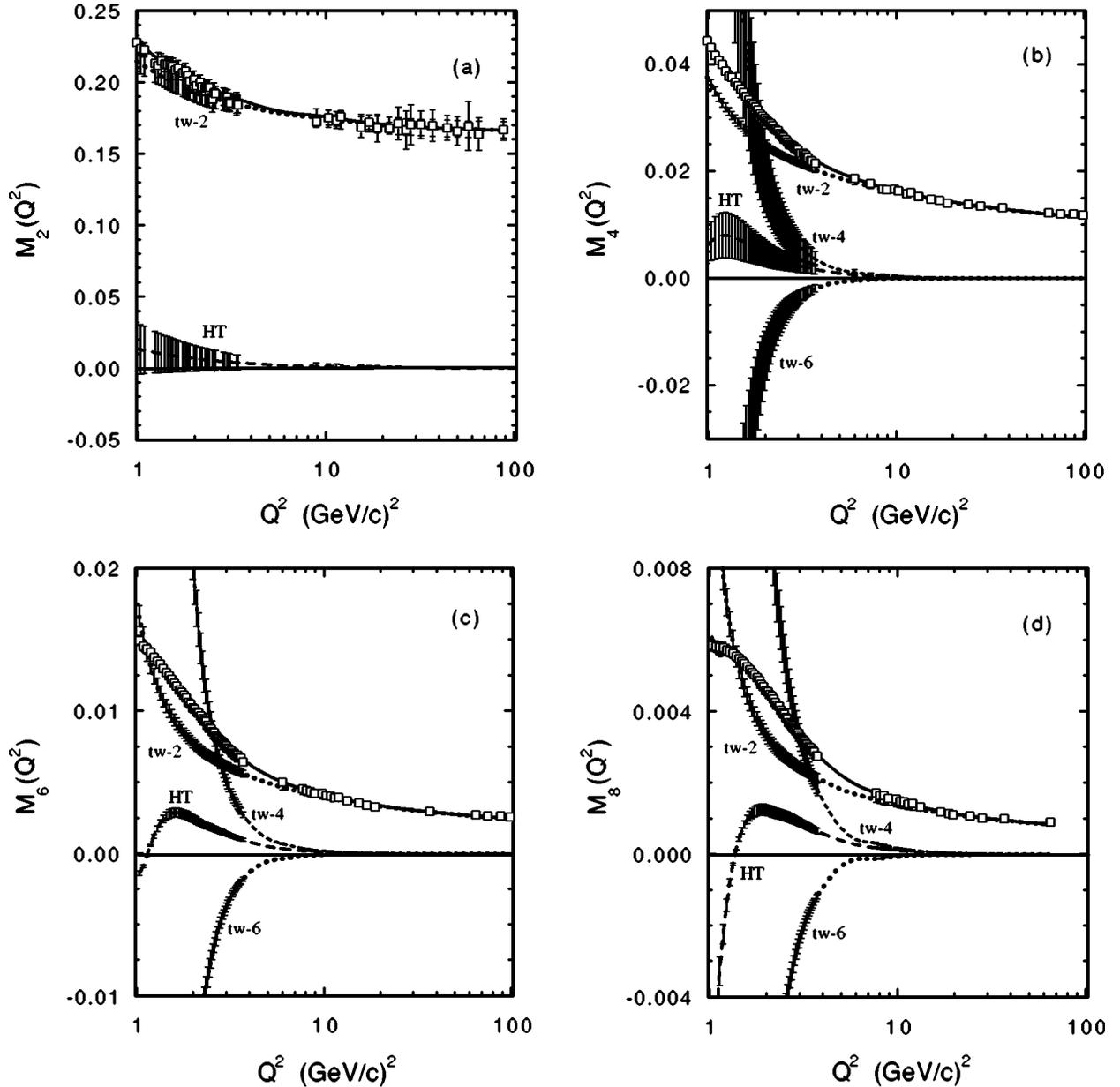
FIG. 11. Results of the twist analysis. The open squares represent the Nachtman moments obtained in this analysis. The solid line is the fit to the moments using Eq. (37) with the parameters listed in Table III. The twist-2, twist-4, twist-6 and higher twist (HT) contributions to the fit are indicated. The twist-2 contribution was calculated using Eq. (39).
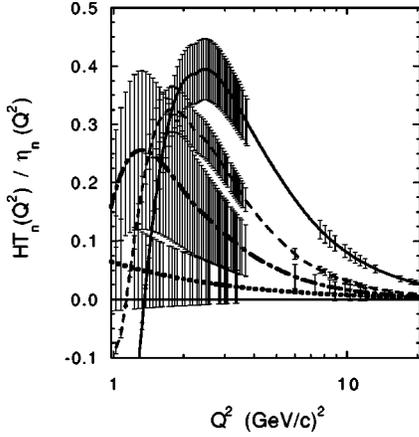
FIG. 12. Ratio of the total higher-twist [see Eq. (38)] to the leading twist given in Eq. (39). Dotted line, M_2; dash-dotted line, M_4; dashed line, M_6; solid line, M_8.

where $\eta_n(Q^2)$ is the leading twist moment and $HT_n(Q^2)$ is the higher-twist contribution given by [53]

$$HT_n(Q^2) = a_n^{(4)} \left[\frac{\alpha_s(Q^2)}{\alpha_s(\mu^2)} \right]^{\gamma_n^{(4)}} \frac{\mu^2}{Q^2} + a_n^{(6)} \left[\frac{\alpha_s(Q^2)}{\alpha_s(\mu^2)} \right]^{\gamma_n^{(6)}} \frac{\mu^4}{Q^4}, \tag{38}$$

where the logarithmic PQCD evolution of the twist-τ contribution is accounted for by the term $[\alpha_s(Q^2)/\alpha_s(\mu^2)]^{\gamma_n^{(\tau)}}$ [corresponding to the Wilson coefficient $E_{n\tau}(\mu, Q^2)$ in Eq. (3)] with an *effective* anomalous dimension $\gamma_n^{(\tau)}$ and the parameter $a_n^{(\tau)}$ [equal to the matrix element $O_{n\tau}(\mu)$ in Eq. (3)] represents the overall strength of the twist-τ term at the renormalization scale $Q^2 = \mu^2$. In Eqs. (37), (38) four higher-twist parameters appear, while the twist-2 moment $\eta_n(Q^2)$ is generally given by the sum of a non-singlet and singlet terms, leading to three unknown parameters, namely the values of the gluon, non-singlet and singlet quark moments at the factorization scale $Q^2 = \mu^2$. However, the decoupling in the PQCD evolution of the singlet quark and gluon densities at large x allows one to consider a pure non-singlet evolution for $n \geq 4$ (cf. [14]). This means that we have only one twist-2 parameter for $n \geq 4$, namely the value of the twist-2 moment $\eta_n(\mu^2)$ at the factorization scale $Q^2 = \mu^2$. The resummation of soft gluons does not introduce any further parameter in the description of the leading twist. Explicitly, for $n \geq 4$ the leading twist moment $\eta_n(Q^2)$ is given by

$$\eta_n(Q^2) = A_n \left[\frac{\alpha_s(Q^2)}{\alpha_s(\mu^2)} \right]^{\gamma_n^{NS}} \left\{ \left[1 + \frac{\alpha_s(Q^2)}{2\pi} C_{DIS}^{(NLO)} \right] e^{G_n(Q^2)} + \frac{\alpha_s(Q^2)}{4\pi} R_n^{NS} \right\}, \tag{39}$$

where the quantities γ_n^{NS}, $C_{DIS}^{(NLO)}$ and R_n^{NS} can be read off from Ref. [16]. In Eq. (39) the function $G_n(Q^2)$ is the key quantity of the soft gluon resummation. At next-to-leading-log it reads as

$$G_n(Q^2) = \ln(n) G_1(\lambda_n) + G_2(\lambda_n) + O[\alpha_s^k \ln^{k-1}(n)], \tag{40}$$

where $\lambda_n \equiv \beta_0 \alpha_s(Q^2) \ln(n) / 4\pi$ and

$$G_1(\lambda) = C_F \frac{4}{\beta_0 \lambda} [\lambda + (1-\lambda)\ln(1-\lambda)],$$

$$\begin{aligned} G_2(\lambda) = &-C_F \frac{4\gamma_E + 3}{\beta_0} \ln(1-\lambda) \\ &- C_F \frac{8K}{\beta_0^2} [\lambda + \ln(1-\lambda)] \\ &+ C_F \frac{4\beta_1}{\beta_0^3} \left[\lambda + \ln(1-\lambda) + \frac{1}{2}\ln^2(1-\lambda) \right], \end{aligned} \tag{41}$$

with $C_F \equiv (N_c^2 - 1)/(2N_c)$, $k = N_c(67/18 - \pi^2/6) - 5N_f/9$, $\beta_0 = 11 - 2N_f/3$, and N_f being the number of active flavors. Note that the function $G_2(\lambda)$ is divergent for $\lambda \to 1$; this means that at large n (i.e. large x) the soft gluon resummation cannot be extended to arbitrarily low values of Q^2. Therefore, for a safe use of present SGR techniques we will work far from the above-mentioned divergences by limiting our analyses of low-order moments ($n \leq 8$) to $Q^2 \geq 1$ $(\text{GeV}/c)^2$.

All the unknown parameters, namely the twist-2 parameter A_n as well as the higher-twist parameters $a_n^{(4)}, \gamma_n^{(4)}, a_n^{(6)}, \gamma_n^{(6)}$, were simultaneously determined from a χ^2-minimization procedure in the Q^2 range between 1 and 100 $(\text{GeV}/c)^2$. In such a procedure only the statistical errors of the experimental moments were taken into account, as well as the updated Particle Data Group value $\alpha_s(M_Z^2) = 0.118$ [54], and a renormalization scale equal to $\mu^2 = 10$ $(\text{GeV}/c)^2$. The uncertainties of the various twist parameters were then obtained by adding the systematic errors to the experimental moments and by repeating the twist extraction procedure. The parameter values are reported in Table III, where it can be seen that the leading twist is determined with a few percent uncertainty, while the precision of the extracted higher twists increases with n reaching an overall 10% for $n = 6$ and 8, thanks to the remarkable quality of the CLAS data at large x. Note that the leading twist is directly extracted from the data, which means that no specific functional shape of the parton distributions is assumed in our analysis. The contribution of higher twists to M_2 was too small to be extracted by the present procedure.

Our results, including the uncertainties for each twist term separately, are reported in Fig. 11 for $n \geq 2$, while the ratio of the total higher-twist contribution to the leading twist is shown in Fig. 12. In addition, the extracted leading twist contribution is reported in Table IV. It can be seen that

(i) the extracted twist-2 term yields an important contribution in the whole Q^2 range of the present analysis;

(ii) the Q^2 behavior of the data leaves room for a higher-twist contribution positive at large Q^2 and negative at $Q^2 \sim 1-2$ $(\text{GeV}/c)^2$; such a change of sign requires in Eq. (38)

TABLE IV. The extracted leading twist contribution $\eta_n(Q^2)$ [see Eq. (39)] shown in Fig. 11, reported with systematic errors.

Q^2 [(GeV/c)^2]	$\eta_2(Q^2)\times 10^{-1}$	$\eta_4(Q^2)\times 10^{-2}$	$\eta_6(Q^2)\times 10^{-2}$	$\eta_8(Q^2)\times 10^{-2}$
1.025	2.13 ± 0.07	3.62 ± 0.09	1.665 ± 0.07	1.223 ± 0.065
1.075	2.11 ± 0.07	3.49 ± 0.09	1.522 ± 0.07	1.022 ± 0.055
1.125	2.09 ± 0.07	3.38 ± 0.08	1.410 ± 0.06	0.883 ± 0.047
1.175	2.08 ± 0.07	3.28 ± 0.08	1.319 ± 0.06	0.781 ± 0.041
1.225	2.07 ± 0.07	3.19 ± 0.08	1.243 ± 0.05	0.704 ± 0.037
1.275	2.05 ± 0.07	3.11 ± 0.08	1.179 ± 0.05	0.643 ± 0.034
1.325	2.04 ± 0.07	3.04 ± 0.07	1.125 ± 0.05	0.593 ± 0.031
1.375	2.03 ± 0.07	2.97 ± 0.07	1.077 ± 0.05	0.553 ± 0.029
1.425	2.02 ± 0.07	2.91 ± 0.07	1.036 ± 0.05	0.519 ± 0.027
1.475	2.01 ± 0.07	2.86 ± 0.07	0.999 ± 0.04	0.490 ± 0.026
1.525	2.00 ± 0.07	2.81 ± 0.07	0.966 ± 0.04	0.465 ± 0.024
1.575	1.99 ± 0.07	2.76 ± 0.07	0.936 ± 0.04	0.443 ± 0.023
1.625	1.98 ± 0.07	2.72 ± 0.07	0.910 ± 0.04	0.424 ± 0.022
1.675	1.97 ± 0.07	2.68 ± 0.07	0.886 ± 0.04	0.407 ± 0.021
1.725	1.96 ± 0.07	2.64 ± 0.06	0.864 ± 0.04	0.392 ± 0.021
1.775	1.95 ± 0.07	2.61 ± 0.06	0.844 ± 0.04	0.378 ± 0.020
1.825	1.95 ± 0.07	2.57 ± 0.06	0.825 ± 0.04	0.366 ± 0.019
1.875	1.94 ± 0.07	2.54 ± 0.06	0.808 ± 0.04	0.355 ± 0.019
1.925	1.93 ± 0.07	2.51 ± 0.06	0.792 ± 0.03	0.344 ± 0.018
1.975	1.93 ± 0.07	2.49 ± 0.06	0.777 ± 0.03	0.335 ± 0.018
2.025	1.92 ± 0.07	2.46 ± 0.06	0.763 ± 0.03	0.326 ± 0.017
2.075	1.91 ± 0.07	2.44 ± 0.06	0.750 ± 0.03	0.318 ± 0.017
2.125	1.91 ± 0.07	2.41 ± 0.06	0.738 ± 0.03	0.311 ± 0.016
2.175	1.90 ± 0.07	2.39 ± 0.06	0.726 ± 0.03	0.304 ± 0.016
2.225	1.90 ± 0.07	2.37 ± 0.06	0.715 ± 0.03	0.298 ± 0.016
2.275	1.89 ± 0.07	2.35 ± 0.06	0.706 ± 0.03	0.292 ± 0.015
2.325	1.89 ± 0.07	2.33 ± 0.06	0.697 ± 0.03	0.287 ± 0.015
2.375	1.89 ± 0.07	2.32 ± 0.06	0.689 ± 0.03	0.283 ± 0.015
2.425	1.88 ± 0.07	2.30 ± 0.06	0.682 ± 0.03	0.279 ± 0.014
2.475	1.88 ± 0.07	2.28 ± 0.06	0.675 ± 0.03	0.275 ± 0.014
2.525	1.88 ± 0.06	2.27 ± 0.06	0.668 ± 0.03	0.271 ± 0.014
2.575	1.88 ± 0.06	2.25 ± 0.06	0.661 ± 0.03	0.267 ± 0.014
2.625	1.87 ± 0.06	2.24 ± 0.05	0.654 ± 0.03	0.264 ± 0.014
2.675	1.87 ± 0.06	2.23 ± 0.05	0.648 ± 0.03	0.260 ± 0.013
2.725	1.87 ± 0.06	2.21 ± 0.05	0.642 ± 0.03	0.257 ± 0.013
2.775	1.87 ± 0.06	2.20 ± 0.05	0.637 ± 0.03	0.254 ± 0.013
2.825	1.86 ± 0.06	2.19 ± 0.05	0.631 ± 0.03	0.251 ± 0.013
2.875	1.86 ± 0.06	2.18 ± 0.05	0.626 ± 0.03	0.248 ± 0.013
2.925	1.86 ± 0.06	2.17 ± 0.05	0.621 ± 0.03	0.245 ± 0.013
2.975	1.86 ± 0.06	2.15 ± 0.05	0.616 ± 0.03	0.243 ± 0.013
3.025	1.85 ± 0.06	2.14 ± 0.05	0.611 ± 0.03	0.240 ± 0.012
3.075	1.85 ± 0.06	2.13 ± 0.05	0.606 ± 0.03	0.238 ± 0.012
3.125	1.85 ± 0.06	2.12 ± 0.05	0.602 ± 0.03	0.236 ± 0.012
3.175	1.85 ± 0.06	2.11 ± 0.05	0.598 ± 0.03	0.233 ± 0.012
3.225	1.85 ± 0.06	2.10 ± 0.05	0.593 ± 0.03	0.231 ± 0.012
3.275	1.84 ± 0.06	2.09 ± 0.05	0.589 ± 0.03	0.229 ± 0.012
3.325	1.84 ± 0.06	2.08 ± 0.05	0.585 ± 0.03	0.227 ± 0.012
3.375	1.84 ± 0.06	2.08 ± 0.05	0.582 ± 0.03	0.225 ± 0.012
3.425	1.84 ± 0.06	2.07 ± 0.05	0.578 ± 0.03	0.223 ± 0.011
3.475	1.84 ± 0.06	2.06 ± 0.05	0.574 ± 0.03	0.221 ± 0.011
3.525	1.84 ± 0.06	2.05 ± 0.05	0.571 ± 0.03	0.220 ± 0.011
3.575	1.83 ± 0.06	2.04 ± 0.05	0.567 ± 0.03	0.218 ± 0.011
3.625	1.83 ± 0.06	2.03 ± 0.05	0.564 ± 0.02	0.216 ± 0.011

TABLE IV. (*Continued*).

Q^2 [(GeV/c)^2]	$\eta_2(Q^2)\times 10^{-1}$	$\eta_4(Q^2)\times 10^{-2}$	$\eta_6(Q^2)\times 10^{-2}$	$\eta_8(Q^2)\times 10^{-2}$
3.675	1.83±0.06	2.03±0.05	0.561±0.02	0.215±0.011
3.725	1.83±0.06	2.02±0.05	0.558±0.02	0.213±0.011
5.967	1.78±0.06	1.79±0.04	0.467±0.02	0.169±0.009
7.268	1.77±0.06	1.72±0.04	0.438±0.02	0.156±0.008
7.645	1.76±0.06	1.70±0.04	0.431±0.02	0.153±0.008
8.027	1.76±0.06	1.68±0.04	0.424±0.02	0.150±0.008
8.434	1.75±0.06	1.66±0.04	0.418±0.02	0.147±0.008
8.857	1.75±0.06	1.65±0.04	0.412±0.02	0.144±0.008
9.781	1.74±0.06	1.61±0.04	0.400±0.02	0.139±0.008
10.267	1.74±0.06	1.60±0.04	0.395±0.02	0.137±0.007
10.793	1.74±0.06	1.58±0.04	0.389±0.02	0.134±0.007
11.345	1.73±0.06	1.57±0.04	0.384±0.02	0.132±0.007
11.939	1.73±0.06	1.55±0.04	0.379±0.02	0.130±0.007
13.185	1.72±0.06	1.52±0.04	0.369±0.02	0.126±0.007
15.310	1.71±0.06	1.48±0.04	0.355±0.02	0.120±0.007
16.902	1.71±0.06	1.46±0.04	0.347±0.02	0.116±0.006
18.697	1.70±0.06	1.43±0.04	0.338±0.01	0.113±0.006
19.629	1.70±0.06	1.42±0.03	0.334±0.01	0.111±0.006
21.625	1.69±0.06	1.40±0.03	0.327±0.01	0.108±0.006
24.192	1.69±0.06	1.37±0.03	0.319±0.01	0.105±0.006
26.599	1.68±0.06	1.35±0.03	0.312±0.01	0.102±0.006
28.192	1.68±0.06	1.34±0.03	0.309±0.01	0.101±0.006
31.858	1.68±0.06	1.32±0.03	0.301±0.01	0.098±0.005
36.750	1.68±0.06	1.29±0.03	0.293±0.01	0.095±0.005
44.000	1.67±0.06	1.26±0.03	0.283±0.01	0.091±0.005
49.750	1.67±0.06	1.24±0.03	0.277±0.01	0.089±0.005
57.000	1.67±0.06	1.22±0.03	0.270±0.01	0.086±0.005
64.884	1.67±0.06	1.20±0.03	0.264±0.01	0.084±0.004
75.000	1.66±0.06	1.17±0.03	0.257±0.01	0.081±0.004
88.000	1.66±0.06	1.15±0.03	0.250±0.01	0.078±0.004
99.000	1.66±0.06	1.13±0.03	0.245±0.01	0.077±0.004

a twist-6 term with a sign opposite to that of the twist-4 term. As already noted in Refs. [14,16], such opposite signs make the total higher-twist contribution smaller than its individual terms;

(iii) the total higher-twist contribution is significant at $Q^2\approx$ few (GeV/c)^2, but it is less than $\simeq 20\%$ of the leading twist for $Q^2 > 5$ (GeV/c)^2.

V. CONCLUSIONS

We extracted the F_2 structure function in a continuous two-dimensional range of Q^2 and x from the inclusive cross section measured with the CLAS detector. Using these data, together with the previously available world data set, we evaluated the Nachtmann moments $M_2(Q^2,x)$, $M_4(Q^2,x)$, $M_6(Q^2,x)$ and $M_8(Q^2,x)$ in the Q^2 range 0.05–100 (GeV/c)^2. The present data set covers a large interval in x, thus reducing the uncertainties in the integration procedure. The Nachtmann moments obtained in this work have been analyzed in terms of a twist expansion in order to simultaneously extract both the leading and the higher twists.

The former has not been treated at fixed order in perturbation theory, but higher-order corrections of PQCD were taken into account by means of soft gluon resummation techniques. Higher twists have been treated phenomenologically by introducing *effective* anomalous dimensions. The range of the analysis was quite large, ranging from 1 to 100 (GeV/c)^2. The leading twist is determined with a few percent uncertainty, while the precision of the higher twists increases with n reaching an overall 10% for $n=6$ and 8, thanks to the remarkable quality of the experimental moments.

The main results of our twist analysis can be summarized as follows: (i) the contribution of the leading twist calculated in the frame of PQCD at NLO remains dominant down to $2Q^2/n\sim 1$ (GeV/c)^2, where n is the moment order. This leads to the conclusion that a PQCD-based description of the proton structure is relevant also at low Q^2, with significant but not crucial corrections. (ii) The total contribution of the multi-parton correlation effects is not negligible for $Q^2 < 5$ (GeV/c)^2 and large x corresponding to the resonance region. This can be seen by comparing the higher twist contribution to M_8, which is more heavily weighted in x, to M_2.

(iii) Different higher twist terms tend to compensate each other in such a way that their sum is small even in a Q^2 region where their absolute contributions exceed the leading twist. This cancellation is responsible for the duality phenomena and leads to the prevailing DIS-inspired picture of photon-proton collisions at low Q^2.

Therefore, we demonstrated that a precise determination of higher twists is feasible with the high quality of the new CLAS data. The main limitation of the present analysis is the use of a phenomenological ansatz for the higher twists. In this respect it is necessary to have better theoretical knowledge of the renormalization group behavior of the relevant higher-twist operators. This would directly test QCD in its non-perturbative regime through the comparison of predictions obtained from lattice simulations with these data.

APPENDIX: FIT OF THE RATIO $R \equiv \sigma_L / \sigma_T$

The function $R(x, Q^2) = \sigma_L / \sigma_T$ was described as

$$
R(x,Q^2) = \begin{cases}
\dfrac{(1-x)^3}{(1-x_{th})^3}\left[\dfrac{0.041\xi_{th}}{\zeta} + \dfrac{0.592}{Q^2} - \dfrac{0.331}{(0.09+Q^4)}\right], & W<2.5, \\[3ex]
\dfrac{0.041\xi}{\zeta} + \dfrac{0.592}{Q^2} - \dfrac{0.331}{(0.09+Q^4)}, & W>2.5.
\end{cases}
\tag{A1}
$$

This parametrization of $R(x, Q^2)$ consists of two different parts: the fit for the DIS region ($W>2.5$ GeV) [55,56] and the function, adjusted to scarce data at small Q^2 [57–59], in the resonance region ($W<2.5$ GeV). The systematic error on this parametrization was estimated according to Ref. [14] as follows:

$$
\delta_R = \begin{cases}
0.08, & W<2.5, \\[3ex]
\dfrac{0.006\xi}{\zeta} + \dfrac{0.01}{Q^2} - \dfrac{0.01}{(0.09+Q^4)}, & W>2.5,
\end{cases}
\tag{A2}
$$

where

$$
\zeta = \log\frac{Q^2}{0.04}, \quad \xi = 1 + 12\frac{Q^2}{1+Q^2}\frac{0.015625}{0.015625+x^2}, \quad \xi_{th} = \xi(W=2.5), x_{th} = x(W=2.5).
\tag{A3}
$$

All dimensional variables are given in GeV.

[1] E. Bloom and F. Gilman, Phys. Rev. Lett. **25**, 1140 (1970); Phys. Rev. D **4**, 2901 (1971).
[2] C.S. Armstrong *et al.*, Phys. Rev. D **63**, 094008 (2001).
[3] A. De Rujula, H. Georgi, and H. Politzer, Ann. Phys. (N.Y.) **103**, 315 (1977).
[4] J.M. Cornwall and R.E. Norton, Phys. Rev. **177**, 2584 (1969).
[5] G. Ricco *et al.*, Phys. Rev. C **57**, 356 (1998).
[6] I. Niculescu *et al.*, Phys. Rev. D **60**, 094001 (1999).
[7] I. Niculescu *et al.*, Phys. Rev. Lett. **85**, 1186 (2000); **85**, 1182 (2000).
[8] P.E. Bosted *et al.*, Phys. Rev. C **51**, 409 (1995).
[9] M.K. Jones *et al.*, Phys. Rev. Lett. **84**, 1398 (2000).
[10] M. Osipenko *et al.*, Report No. CLAS-NOTE-2003-001, 2003.
[11] O. Nachtmann, Nucl. Phys. **B63**, 237 (1973).
[12] R.G. Roberts, *The Structure of the Proton* (Cambridge University Press, Cambridge, England, 1990).
[13] M. Beneke, Report No. CERN-TH/98-233; M. Maul *et al.*, Phys. Lett. B **401**, 100 (1997); M. Dasgupta and B.R. Webber, *ibid.* **382**, 273 (1996); E. Stein *et al.*, *ibid.* **376**, 177 (1996).
[14] G. Ricco *et al.*, Nucl. Phys. **B555**, 306 (1999).
[15] S. Catani *et al.*, Report No. CERN-TH/96-86; M. Cacciari and S. Catani, Report No. CERN-TH/2001-174.

[16] S. Simula, Phys. Lett. B **493**, 325 (2000).

[17] M.D. Mestayer *et al.*, Nucl. Instrum. Methods Phys. Res. A **449**, 81 (2000).

[18] E.S. Smith *et al.*, Nucl. Instrum. Methods Phys. Res. A **432**, 265 (1999).

[19] G. Adams *et al.*, Nucl. Instrum. Methods Phys. Res. A **465**, 414 (2001).

[20] M. Amarian *et al.*, Nucl. Instrum. Methods Phys. Res. A **460**, 460 (2001).

[21] A. Bodek *et al.*, Phys. Rev. D **20**, 1471 (1979).

[22] S. Stein *et al.*, Phys. Rev. D **12**, 1884 (1975).

[23] P. Bosted (private communication).

[24] D. Wiser, Ph.D. thesis, University of Wisconsin, 1977.

[25] L.W. Mo and Y.S. Tsai, Rev. Mod. Phys. **41**, 205 (1969); Yung-Su Tsai, Phys. Rev. **122**, 1898 (1961).

[26] http://improv.unh.edu/Maurik/gsim_info.shtml

[27] I. Akushevich *et al.*, Acta Phys. Pol. B **28**, 563 (1997).

[28] S.I. Bilenkaya *et al.*, JETP Lett. **19**, 317 (1974).

[29] F.W. Brasse *et al.*, Nucl. Phys. **B110**, 413 (1976).

[30] A.C. Benvenuti *et al.*, Phys. Lett. B **223**, 485 (1989).

[31] M.R. Adams *et al.*, Phys. Rev. D **54**, 3006 (1996).

[32] M. Arneodo *et al.*, Nucl. Phys. **B483**, 3 (1997).

[33] I. Abt *et al.*, Nucl. Phys. **B407**, 515 (1993).

[34] T. Ahmed *et al.*, Nucl. Phys. **B439**, 471 (1995).

[35] T. Ahmed *et al.*, Nucl. Phys. **B470**, 3 (1996).

[36] C. Adloff *et al.*, Nucl. Phys. **B497**, 3 (1997).

[37] C. Adloff *et al.*, Report No. DESY-99-107, 1999.

[38] M. Derrick *et al.*, Phys. Lett. B **316**, 412 (1993).

[39] M. Derrick *et al.*, Z. Phys. C **65**, 379 (1995).

[40] M. Derrick *et al.*, Z. Phys. C **69**, 607 (1995).

[41] M. Derrick *et al.*, Z. Phys. C **72**, 399 (1996).

[42] J. Brietweg *et al.*, Phys. Lett. B **407**, 432 (1997).

[43] J. Brietweg *et al.*, Eur. Phys. J. C **7**, 609 (1999).

[44] L.W. Whitlow *et al.*, Phys. Lett. B **282**, 475 (1992).

[45] M. Mestayer, Report No. SLAC-214, 1978; W.B. Atwood *et al.*, Phys. Lett. **64B**, 479 (1976); E.M. Riordan *et al.*, Report No. SLAC-PUB-1634, 1975; A. Bodek *et al.*, Phys. Rev. Lett. **30**, 1087 (1973); J.S. Poucher *et al.*, *ibid.* **32**, 118 (1974); G. Miller, Phys. Rev. D **5**, 528 (1972); E.D. Bloom *et al.*, Report No. SLAC-PUB-653, 1971; M. Breidendach, Report No. MIT-2098-635, 1970.

[46] http://wwwinfo.cern.ch/asd/cernlib/overview.html

[47] J.J. Aubert *et al.*, Nucl. Phys. **B259**, 189 (1985).

[48] A. Milsztajn *et al.*, Z. Phys. C **49**, 527 (1991).

[49] D. Allasia *et al.*, Z. Phys. C **28**, 321 (1991).

[50] F.W. Brasse *et al.*, Report No. DESY-67-34, 1967; W. Albrecht *et al.*, Phys. Lett. **28B**, 225 (1968); W. Albrecht *et al.*, Nucl. Phys. **B13**, 1 (1969).

[51] B. Adeva *et al.*, Phys. Rev. D **58**, 112001 (1998).

[52] S. Forte *et al.*, J. High Energy Phys. **05**, 062 (2002).

[53] X. Ji and P. Unrau, Phys. Rev. D **52**, 72 (1995); U.K. Yang and A. Bodek, Phys. Rev. Lett. **82**, 2467 (1999).

[54] Particle Data Group, D.E. Groom *et al.*, Eur. Phys. J. C **15**, 1 (2000).

[55] L.W. Whitlow *et al.*, Phys. Lett. B **250**, 193 (1990).

[56] J. Bartelski *et al.*, hep-ph/9804415.

[57] V. Burkert, Report No. CEBAF-PR-93-035, 1993.

[58] J. Drees *et al.*, Z. Phys. C **7**, 183 (1981).

[59] L.M. Stuart *et al.*, Phys. Rev. D **58**, 032003 (1998).